coatings

Article

Assessment of New Imidazol Derivatives and Investigation of Their Corrosion-Reducing Characteristics for Carbon Steel in HCl Acid Solution

Ahmed Fatah [1], Nadia Timoudan [2], Mohamed Rbaa [3], Fouad Benhiba [1,2,*], Rachid Hsissou [4], Zaki S. Safi [5], Ismail Warad [6], Abeer A. AlObaid [7], Basheer M. Al-Maswari [8], Amale Boutakiout [2], Hassan Zarrok [1], Brahim Lakhrissi [3], Abdelkabir Bellaouchou [2], Charafeddine Jama [9], Fouad Bentiss [9,10], Hassan Oudda [1] and Abdelkader Zarrouk [2,*]

1 Laboratory of Advanced Materials and Process Engineering, Faculty of Sciences, Ibn Tofail University, P.O. Box 133, Kenitra 14000, Morocco; fataha47@gmail.com (A.F.); hzarrok@gmail.com (H.Z.); ouddahassan@gmail.com (H.O.)
2 Laboratory of Materials, Nanotechnology and Environment, Faculty of Sciences, Mohammed V University in Rabat, P.O. Box 1014, Rabat 10000, Morocco; nadia.timoudan1995@gmail.com (N.T.); amale.boutakiout@gmail.com (A.B.); a.bellaouchou@um5r.ac.ma (A.B.)
3 Laboratory of Organic Chemistry, Inorganic, Electrochemistry, and Environment, Department of Chemistry, Faculty of Sciences, Ibn Tofail University, P.O. Box 133, Kenitra 14000, Morocco; mohamed.rbaa10@gmail.com (M.R.); b.lakhrissi2012@gmail.com (B.L.)
4 Laboratory of Organic Chemistry, Bioorganic and Environment, Chemistry Department, Faculty of Sciences, Chouaib Doukkali University, P.O. Box 20, El Jadida 24000, Morocco; r.hsissou@gmail.com
5 Chemistry Department, Faculty of Science, Al Azhar University-Gaza, Gaza P.O. Box 1277, Palestine; zaki.safi@gmail.com
6 Department of Chemistry, AN-Najah National University, Nablus P.O. Box 7, Palestine; i.kh.warad@gmail.com
7 Department of Chemistry, College of Science, King Saud University, P.O. Box 2455, Riyadh 11451, Saudi Arabia; aaalobaid@ksu.edu.sa
8 Department of Chemistry, Yuvaraja's College, University of Mysore, Mysuru 570005, India; basheer.almaswari@gmail.com
9 Univ. Lille, CNRS, INRAE, Centrale Lille, UMR 8207-UMET-Unité Matériaux et Transformations, F-59000 Lille, France; charafeddine.jama@centralelille.fr (C.J.); fbentiss@gmail.com (F.B.)
10 Laboratory of Catalysis and Corrosion of Materials, Faculty of Sciences, Chouaib Doukkali University, P.O. Box 20, El Jadida 24000, Morocco
* Correspondence: fouad.benhiba@uit.ac.ma (F.B.); azarrouk@gmail.com (A.Z.)

Citation: Fatah, A.; Timoudan, N.; Rbaa, M.; Benhiba, F.; Hsissou, R.; Safi, Z.S.; Warad, I.; AlObaid, A.A.; Al-Maswari, B.M.; Boutakiout, A.; et al. Assessment of New Imidazol Derivatives and Investigation of Their Corrosion-Reducing Characteristics for Carbon Steel in HCl Acid Solution. *Coatings* **2023**, *13*, 1405. https://doi.org/10.3390/coatings13081405

Academic Editor: Yanxin Qiao

Received: 10 July 2023
Revised: 31 July 2023
Accepted: 3 August 2023
Published: 10 August 2023

Abstract: This study assessed the corrosion inhibitory and adsorption properties of two imidazol derivatives, namely 5-((2,4,5-triphenyl-1H-imidazol-1-yl)methyl)quinolin-8-ol (TIMQ) and 5-((2-(4-chlorophenyl)-4,5-diphenyl-1H-imidazol-1-yl)methyl)quinolin-8-ol (CDIQ), on carbon steel (CS) in 1 M of HCl using electrochemical methods, including electrochemical impedance spectroscopy (EIS), potentiodynamic polarization measurements (PDP), UV–visible spectroscopy (UV–v), scanning electron microscopy (SEM), and molecular modeling. The findings showed that TIMQ and CDIQ were potent inhibitors with inhibition efficiencies of 94.8% and 95.8%, respectively. The potentiodynamic polarization experiments showed that the inhibitors worked as mixed-type inhibitors, and the impedance investigations supported the improvement of a protective layer for the inhibitor on the metal surface. Each inhibitor was adsorbed onto the carbon steel surfaces, according to the Langmuir adsorption method. The steel was shielded from acidic ions by an adsorbed coating of the inhibitor molecules, according to SEM. Density functional theory (DFT) calculations and molecular dynamics (MD) simulations were used to inspect the results, and a good correlation was found between these results and those of the study. This information can be applied to determine the effectiveness of inhibitors in a HCl acid solution.

Keywords: imidazol analogs; corrosion inhibition; PDP/EIS; SEM/EDS/UV–v; DFT/dynamics

1. Introduction

The nemesis of many industrial fields is corrosion. According to certain estimates, corrosion destroys over 150 million tons of steel annually, or approximately a fourth of the total amount produced [1]. This industrial blight can appear in a variety of ways, from straightforward uniform corrosion to more intricate characteristics found in tough industrial situations. The remedies differ depending on the industrial sectors, and whichever remedy is selected is always the product of a technological, environmental, and frequently economic compromise. Utilizing corrosion inhibitors is one of the most practical and effective ways to prevent corrosion [2–6].

Metallic corrosion is thought to be effectively inhibited by organic inhibitors containing aromatic rings, multiple bonds, and heteroatoms (N, S, and O) in the form of polar functional groups [7–12]. Their adsorption (electron-rich) centers adhere to the metal's surface, preventing corrosion. Metal corrosion inhibition can vary according to the particular type of metal and the properties of the inhibitor compounds. They may bind to metal surfaces through physisorption, chemisorption, or both [13,14]. Due to their higher chelating activity and reduced electronegativity, compounds containing nitrogen demonstrated effective protection levels [15,16]. However, due to the variety of heterocyclic compounds, creating green and highly effective corrosion inhibitors is a significant challenge.

Utilizing efficient computational chemistry methods such as the DFT, it is possible to employ the quantum chemical principle to explain the reactivity and anticorrosive behavior of the inhibitor compounds [17–24]. Computational chemistry was used in the current study to confirm and complete the experimental results for correlating the corrosion efficiencies of the two investigated inhibitors using calculated quantum global and local chemical reactivity indices and to elucidate the mechanism of the studied compounds anticorrosive effect.

This study is original in that it examines the inhibitory action of two synthetic imidazol analogs, i.e., TIMQ and CDIQ, as effective corrosion inhibitors for CS in 1 M HCl media. The inhibiting effects of TIMQ and CDIQ on the corrosion of CS in 1 M HCl were examined using PDP, EIS, UV–v, and SEM. A quantum chemical analysis was used to assess the relationship between the chemical structure and the inhibitory effects of the two imidazole analogues.

The advantages of TIMQ and CDIQ is that they are fully soluble, easy to prepare, inexpensive, and have a low toxicity. Examining their anticorrosive properties is important in the current context to synthesize inhibitors with a low environmental impact.

The information on the anticorrosive properties of some important imidazole analogue derivatives in 1 M of hydrochloric acid for carbon steel are listed in the Table 1. The efficiencies presented in this table are lower than those of the two studied inhibitors, TIMQ (94.8%) and CDIQ (95.8%), which is an added advantage for the present study.

Table 1. Anticorrosive properties of some important imidazole analogue derivatives in 1 M of hydrochloric acid for CS.

Imidazole Analogue Derivatives	Anticorrosive Properties (%)	References
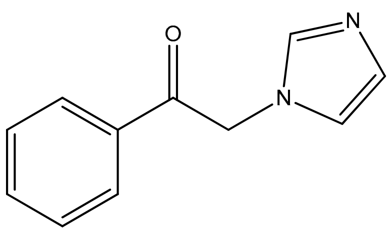 2-(1H-imidazol-1yl)-1-phenylethanone (Im1)	91.87	[25]

Table 1. *Cont.*

Imidazole Analogue Derivatives	Anticorrosive Properties (%)	References
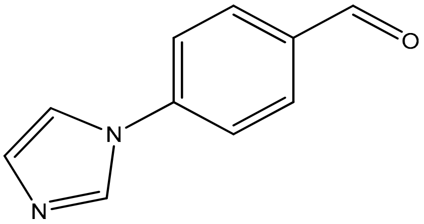 4-(1H-imidazol-1-yl)benzaldehyde (Im2)	92.21	[25]
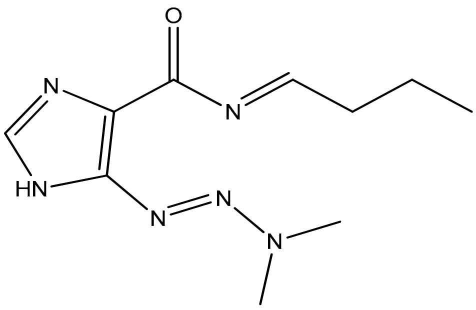 N-(Butylidene)-5-(3,3-Dimethyltriaz-1-en-1-yl)-1H-Imidazole-4-Carboxamide (Im3)	89.00	[26]
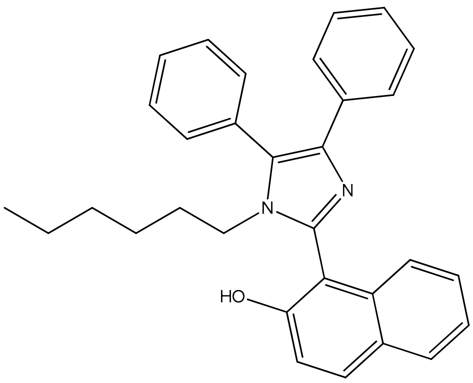 2-(2-hydroxynaphthalen-1-yl)-4,5-diphenyl-1-hexyl-1H-imidazole(Im4)	91.80	[27]

2. Experiment

2.1. Materials

The iron alloy under investigation, known as CS, was composed of the following elements (in weight percentages): 0.370% C, 0.680% Mn, 0.059% Ni, 0.009% Co, 0.160% Cu, 0.016% S, 0.011% Ti, 0.230% Si, 0.077% Cr, and the rest iron. For electrochemical testing, the CS surface samples were exposed at 1 cm^2 in the acid solution. The CS substrates were prepared prior to use. They were polished with a range of grains, degreased with acetone, cleaned with distilled water, and then dried in an air dryer. The ASTM standardization was applied to the CS surface preparation [28]. In order to create the 1 M HCl solution, 37% hydrochloride acid was diluted with distilled water. The structures of both compounds used in this study are illustrated in Figure 1.

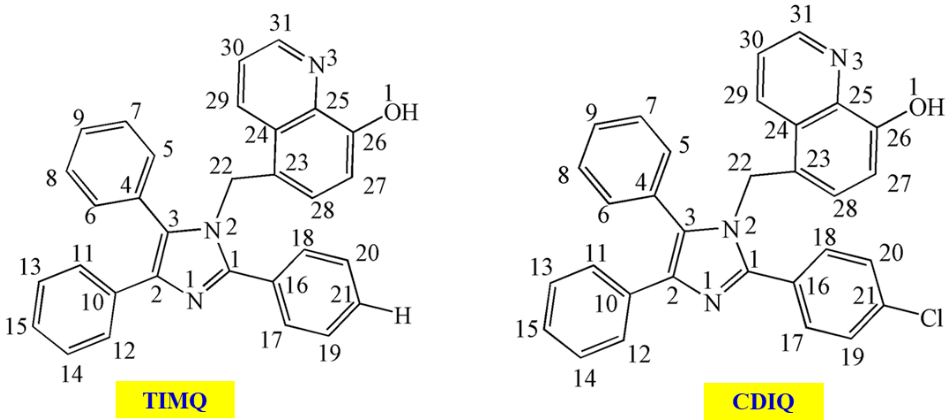

Figure 1. Chemical structure of the imidazol analogs.

2.2. Electrochemical Analysis

To study the corrosion inhibition, electrochemical tests were conducted using a conventional three-electrode cell. This consisted of a small 1 cm^2 CS surface as the working electrode, a saturated calomel electrode (SCE), and a platinum wire as the reference and counter electrode. The test was then associated with a PGZ100-type potentiostat, and all the experiments were conducted in a constant temperature environment in a thermostatic bath, and underwent a 30-min immersion period to reach a balanced open-circuit potential (OCP). The PDP tests were performed using a 5×10^{-4} V s^{-1} sweep rate from -8×10^2 mV to -1×10^2 mV/OCP. The definition of the inhibitory action ($\eta_{TF}(\%)$) is as follows.

$$\eta_{TF}(\%) = \left(\frac{i_{corr,^\circ} - i_{corr}}{i_{corr,^\circ}} \right) \times 100\% \quad (1)$$

where $i_{corr,^\circ}$ and i_{corr} represent the corrosion current densities in the presence and absence of the imidazol analogs, respectively.

Steady-state electrochemical impedance spectroscopy was performed using the AC signal in a frequency interval from 100 kHz to 10 mHz at an amplitude of 10 mV. The following equation provides the inhibitory efficiency using the Nyquist plots' forms.

$$\eta_{EI}(\%) = \left(\frac{R_{P,i} - R_{P,^\circ}}{R_{P,i}} \right) \times 100\% \quad (2)$$

where $R_{P,i}$ and $R_{P,^\circ}$ represent the polarization resistance with and without the imidazole analogs, respectively.

To ensure the results were reliable and reproducible, the measurements were conducted three times for each experimental trial, and the average values were then reported.

In the absence of TIMQ and CDIQ, we used the previously published results from our team for both the stationary and transitory techniques regarding the effect of the temperature and concentration. These experiments were conducted under similar circumstances [29].

2.3. SEM Analysis

The SEM equipment (JEOL-JSM-IT-100, JEOL, Akishima, Tokyo) was used to analyze the surface morphology and energy-dispersive X-Ray spectroscopy (EDS) (Thermo Fisher, Waltham, MA, USA) of the CS samples. The plates were placed in a 1 M HCl bath at 303 K with and without the addition of the TIMQ and CDIQ inhibitors and maintained for 24 h. We used the SEM results that our team had previously released in the absence of inhibitors, which were performed under identical conditions. These works were almost immediately submitted for publication.

2.4. UV–Visible Analysis

Using a JASCO V-700-type device (Thermo Fisher, Waltham, MA, USA), the corrosive solutions generated by immersing the plate in the corrosive environment both without and with the TIMQ and CDIQ inhibitors at concentrations of 10^{-3} M were analyzed.

2.5. DFT and MD Details

We attempted to understand the mechanism of the effect of imidazol analogues on CS surfaces by using the DFT procedure in an aqueous phase [30]. This theoretical adaptation also allowed for the prognosticated experimental inhibitory efficacy of the neutral and protonated imidazol analogs to be reconciled with the chemical reactivity indices [31]. The DFT method using the Becke three-parameter Lee–Yang–Parr (B3LYP) hybrid functional [32–37] was performed to optimize the geometrical structure of the two investigated inhibitors in the depicted neutral and non-charged forms. The 6-31+G(d,p) basis set was employed to conduct the optimization process. The geometry of the optimization approach was realized in aqueous phases utilizing the polarizable continuum model (PCM) at similar levels of theory as the electrochemical corrosion that occurred in the H_2O phase [38]. The absence of fictitious frequencies demonstrated the minima of these substrates' potential energy surfaces. All the calculations were conducted using the Gaussian-09 software [39]. All the molecules were assembled with the help of Gaussview [40], a program that provides graphs of molecular orbitals, including the highest occupied molecular orbital (HOMO) and the lowest unoccupied molecular orbital (LUMO), as well as a graphical representation of the molecular electrostatic potentials. It is vital to note that the B3LYP approach has been frequently used in the literature to research electrical characteristics, predict chemical reactivity, and explore the anticorrosive effects of inhibitor chemicals [17,19,41–45].

The energy gap (ΔE) of the analyzed inhibitors was determined by subtracting the HOMO (E_H) and LUMO (E_L) energy levels as $\Delta E = E_H - E_L$. The relativities between the inhibitors and the metal surface (ΔE_1 and ΔE_2) were evaluated as follows.

$$\Delta E_1 = E_H^{inh} - E_H^{Fe}, \text{ and } \Delta E_2 = E_H^{Fe} - E_H^{inh} \quad (3)$$

where E_H^{inh} is the energy HOMO of inhibitor and $E_H^{Fe} = -7.9024$ and $E_L^{Fe} = -0.0151$ eV are the energies of the HOMO and LUMO of the iron metal, respectively [46]. The main global reactivity descriptors (GRDs), such as the fundamental deviation (F_g), global hardness for inhibitor (η_{inh}) and iron (η_{Fe}), softness (S), electronegativity inhibitor (χ_{inh}), and electrophilicity (ω) using the vertical ionization potential (I_v) and vertical electron affinity (A_v), were used to assess the report of the transferred electrons (ΔN_{110}) and electron back-donation energy (ΔE_{b-d}) [29,47–53].

$$I_\nu \approx E(N-1) - E(N),\ A_\nu \approx E(N) - E(N+1), \text{ and } F_g = I_\nu - A_\nu \quad (4)$$

$$\chi = \frac{1}{2}(I_\nu + A_\nu),\ \eta = \frac{1}{2}(I_\nu - A_\nu),\ S = \frac{1}{\eta},\ and\ \omega = \frac{\chi^2}{2\eta} \quad (5)$$

$$\Delta N = \frac{\Phi_{Fe} - \chi_{inh}}{2(\eta_{Fe} + \eta_{inh})} \text{ and } \Delta E_{b-d} = -\frac{\eta_{inh}}{4} \quad (6)$$

$E(N)$, $E(N-1)$, and $E(N+1)$ stand for the overall energies of the optimized structures in the above equations at neutral, cations, and anions geometries, respectively.

The work function and hardness of *Fe*(110) are, respectively, Φ_{Fe} = 4.82 eV and η_{Fe} = 0. Assuming that $I = A$ for CS, η_{Fe} was equal to 0 eV [54]. The inhibitor's electronegativity and hardness are represented by the letters "χ_{inh}" and "η_{inh}", respectively. The adsorption of an inhibitor compound (adsorbate) on the *Fe* surface (adsorbent) adsorbent is favored by suitable centers such as heteroatoms (N and O atom), as well as the π-electrons of the delocalized rings. Therefore, to obtain information on the site where adsorption occurs, an analysis of the electronic parameters of the active centers (LRDs) was performed in terms of the Fukui functions [55,56]. The condensed Fukui indices were applied to identify the atoms of the examined inhibitors that were most sensitive to electrophilic and/or nucleophilic attacks (f_A^+ and f_A^-, respectively). A finite difference approximation calculated the indices using the following formulas.

$$f_A^+ = q_A(N+1) - q_A(N) \text{ (for nucleophilic attacks)} \quad (7)$$

$$f_A^- = q_A(N) - q_A(N-1) \text{ (for electrophilic attacks)} \quad (8)$$

where $q_A(N)$, $q_A(N+1)$, and $q_A(N-1)$ are the Hierfield charges for the neutral, anion, and cation electron systems, respectively. The Multiwfn program [57] was applied to extract the Fukui functions and their dual descriptors. The following algorithm can be used to quickly determine the local condensed softness (σ_k^α) and the local electrophilicity indices (ω_k^α), which are useful for comparing the reactivity of identical atoms in other compounds.

$$\sigma_A^\pm = S \times f_k^\alpha \; and \; \omega_k^\pm = \omega \times f_k^\pm \quad (9)$$

where σ_A^+, σ_A^-, ω_k^+, and ω_k^- reflect the local softness and electrophilicity corresponding to nucelophilic (+) and electrophilic (−) attacks, respectively.

To state it more precisely, the dual Fukui indices offer a straightforward and perceptible way to comprehend the dual local philicity ($\Delta\omega_k$) and the chemical reactivity in a local method, also known as the second order Fukui functions (f_k^2, the associated dual local softness ($\Delta\sigma_k$). The following is a definition of these dual descriptors [58–60].

$$f_k^2 = f_k^+ - f_k^-, \; \Delta\sigma_A = \sigma_A^+ - \sigma_A^- \text{ and } \Delta\omega_A = \omega_A^+ - \omega_A^- \quad (10)$$

MD simulations were used to examine how TIMQ and CDIQ interacted with the *Fe*(110) systems. This approach was produced via the Materials Studio/2016 program Forcite module [61,62]. A simulation box (27.30 × 27.30 × 37.13 Å^3) with an 11 × 11 unit cell was used to simulate the particle movements (500H_2O, 5H_3O^+, 5Cl^-, and imidazol analogs) within the simulation box with a 27.13 Å^3 vacuum at a temperature of 303 K controlled by the Andersen thermostat in the constant number (N), constant volume (V), and constant temperature (T) (NVT) ensemble, a simulation time of 1000 ps, and a time step of 1.0 fs [63].

3. Results and Discussion

3.1. PDP Investigation

The PDP method was used to evaluate the influence of the varying concentrations of two studied inhibitors, namely TIMQ and CDIQ, on the corrosion behavior of steel in a 1M HCl solution at 298 K. The anodic and cathodic slopes (β_a and β_c), as well as the corrosion current density (i_{corr}), corrosion potential (E_{corr}), inhibitory efficiency (IE%), and other electrochemical characteristics collected from the PDP tests are examined in Figure 2 and Table 2, respectively. Figure 2 illustrates the PDP plots of five concentrations of the inhibitors (TIMQ and CDIQ) for steel in 1M of HCl. The corrosion current densities i_{corr} within the varying concentrations of TIMQ and CDIQ molecules decreased as the concentration of the TIMQ and CDIQ molecules increased, providing excellent inhibitory efficiencies at an optimal concentration (10^{-3} M) for the two studied molecules (TIMQ and CDIQ) [64,65]. In addition, the higher inhibition efficiencies of the two studied molecules TIMQ and CDIQ (potent inhibitors) were 94.8 and 95.2%, respectively. Furthermore, increasing the concentrations of the two studied inhibitors led to the formation of a layer that further reduced the rate of corrosion due to the attack of chloride ions in the electrolytic medium with the good inhibition efficiency [66,67]. As illustrated in Table 2, the CDIQ inhibitor presented a higher inhibition efficiency compared to the TIMQ molecule. In addition, the displacement of the corrosion potential values for the two studied TIMQ and CDIQ molecules compared to the 1 M HCl solution alone were essentially less than 85 mV/SCE. Thus, the two investigated molecules (TIMQ and CDIQ) inhibited both anodic and cathodic reactions associated with the corrosion of steel in an acidic medium, and were suggested to be mixed-type inhibitors [22,62,68–70]. Additionally, the anodic and cathodic Tafel slope (β_a and β_c) values changed in the existence of four concentrations of the two investigated molecules, which reflected the effects of the TIMQ and CDIQ molecules on the kinetics of the anodic and cathodic mechanism.

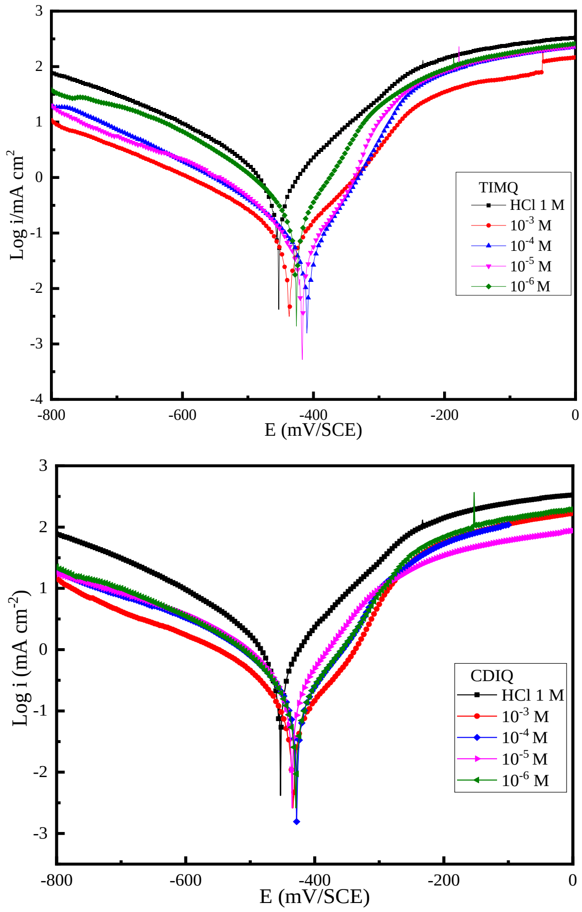

Figure 2. PDP of MS in a 1 M HCl medium with four concentrations of inhibitors (TIMQ and CDIQ) at 303 K.

Table 2. PDP characteristics for CS in an electrolytic medium at 303 K, both unfettered and inhibited with varying quantities of two molecules (TIMQ and CDIQ).

Inhibitors and Corrosive Solution	Conc. (M)	$-E_{corr}$ (mV/SCE)	i_{corr} (µA cm^{-2})	$-\beta_c$ (mV dec^{-1})	β_a (mV dec^{-1})	η_{TF}(%)
HCl	1	456.3	1104.1	155.4	112.2	-
TIMQ	10^{-6}	430.4	239	82.5	53.5	78.3
	10^{-5}	442.6	90.5	78.1	123.9	91.8
	10^{-4}	417.8	81.2	111.2	62.0	92.6
	10^{-3}	389.4	57.2	111.3	52.8	94.8
CDIQ	10^{-6}	430.3	166.1	166.1	91.9	68.6
	10^{-5}	423.2	135.3	55.8	51.8	87.7
	10^{-4}	427.7	104.2	77.5	69.6	90.5
	10^{-3}	433.4	52.1	62.0	76.6	95.2

3.2. EIS Investigation

Figures 3 and 4 illustrate the data obtained from the EIS, Bode, and phase angle for CS in the existence and absence of TIMQ and CDIQ using varying concentrations of the two studied inhibitory molecules in an electrolytic medium at 303 K, respectively. As illustrated in Figure 3, the diameter of the impedance of the two investigated molecules

(TIMQ and CDIQ) at four concentrations was higher compared to the 1M HCl alone. Therefore, the two tested molecules had a strong protection influence against corrosion on the steel electrode [71–73]. The Bode curves (Figure 4) also revealed a time constant that was a low-frequency surface double layer. Figure 5 displays the equivalent circuit (EC) employed to interpret the Nyquist and Bode curves. The terms "R_S", "CPE", and "R_{ct}" stand for the "solution resistance", "constant phase element" (or "CPE_{dl}", which refers to the double layer), and "charge transfer impedance", respectively. Due to the influence of surface heterogeneities on the dispersion, molecule adsorption, and formation of porous layers, the CPE constant phase element was utilized in place of the capacitor, since, the anticorrosive behavior of an electric double layer capacitor was not the same as the pure capacitance [74–76]. Additionally, the impedance of the CPE was calculated according to Equation (11).

$$Z_{CPE} = Q^{-1} \times (i \times \omega)^{-n} \quad (11)$$

where ω, Q, i, and n are the angular frequency, the proportionality coefficient, the imaginary unit, and the surface irregularity that determine when the imaginary portion of the impedance achieves its greatest value. The values of the constant phase element (CPE, Q:charge and n: surface irregularity), which reflects the capacitance of the electric double layer (C_{dl}), adsorption inhibitor film, Rs the resistance of the solution, and R_P the resistance for polarization are also determined using Equation (12).

$$C_{dl} = \sqrt[n]{Q \times R_P^{1-n}} \quad (12)$$

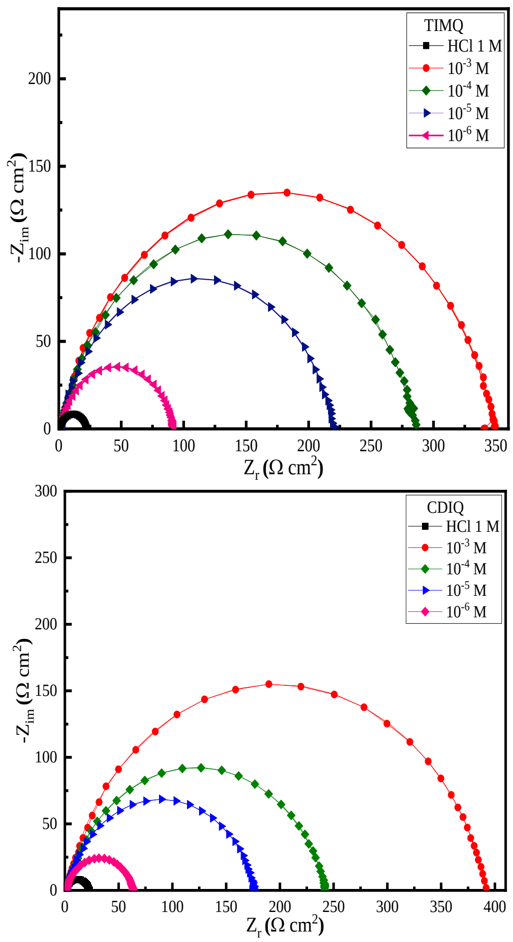

Figure 3. EIS of CS in a 1 M HCl medium with four concentrations of the inhibitors TIMQ and CDIQ at 303 K.

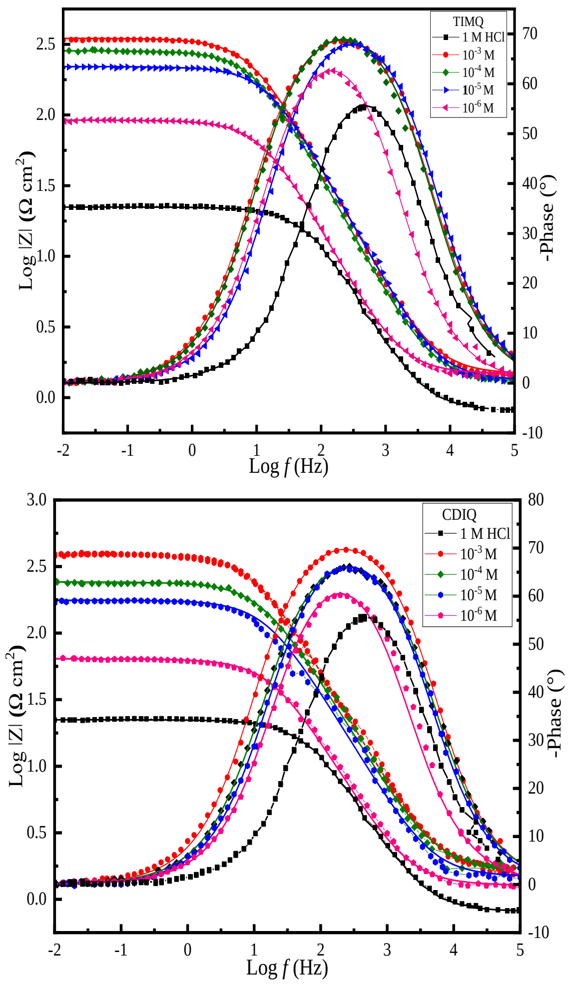

Figure 4. EIS (Bode and phase angle plots) of a 1 M HCl medium with four concentrations of the inhibitors TIMQ and CDIQ at 303 K.

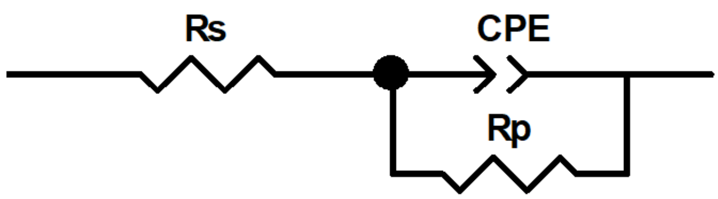

Figure 5. Diagram of the equivalent circuit used to fit the impedance spectra.

The corrosion protection was investigated and addressed based on the charge transfer resistance measurements. Additionally, the performance of the CS electrode as a corrosion inhibitor improved in direct proportion to the R_{ct} value. According to the results analyzed and compiled in Table 3, the same Rs values indicated the similarity of the electrolyte conductivity. According to the findings examined and discussed in Table 3, the CS immersed in an aggressive medium exhibited the lowest R_{ct} value, which indicated a low corrosion resistance. Additionally, since the R_{ct} was low, the ion diffusion rate was high under the vacuum conditions [77–79]. This outcome caused a layer to build on the CS electrode surface. Additionally, in the existence of the ideal concentration of CDIQ, the charge transfer resistance values for carbon steel surfaces were higher than those in the absence of TIMQ, and its inhibitory efficiency also increased. This result was confirmed by the results obtained in the PDP study. In addition, for the steel electrode surface, the C_{dl} values decreased as the concentrations of the two studied molecules increased, compared to the pure 1M HCl solution, due to a decrease in the dielectric constant or an increase in the thickness of the surface layer [71,80–82]. Due to the differences in the surface finish of the steel electrode, the influence of the metal structure and surface on corrosion was greater, leading to increased protection.

Table 3. EIS parameters for the steel electrode uninhibited and inhibited with four concentrations of the investigated molecules (TIMQ and CDIQ) in an electrolytic medium at 303 K.

Medium	Conc. (M)	R_s (Ω cm^2)	R_p (Ω cm^2)	$10^6 \times Q$ (μF s^{n-1} cm^{-2})	n	C_{dl} (μF cm^{-2})	χ^2	η_{EI}(%)
HCl	1	0.83	21.57	293.9	0.845	116.2	0.002	-
TIMQ	10^{-3}	1.45	343.3	77.7	0.871	45.5	0.008	93.8
	10^{-4}	1.25	283.3	91.9	0.868	52.8	0.008	92.4
	10^{-5}	2.13	218.8	101.2	0.860	54.4	0.009	90.1
	10^{-6}	1.31	90.54	90.5	0.851	84.7	0.009	76.2
CDIQ	10^{-3}	1.64	390.1	66.7	0.871	38.8	0.009	94.4
	10^{-4}	1.66	240.7	80.4	0.861	42.6	0.009	91.1
	10^{-5}	1.39	175.1	103.2	0.852	51.4	0.009	87.7
	10^{-6}	1.17	62.1	251.7	0.846	118.0	0.009	65.3

3.3. Temperature Effect and Kinetic Parameters

To identify the interaction mechanism between the studied inhibitory compounds and the metallic surface, a temperature effect was investigated at four temperatures in a corrosive environment (Figure 6). The stationary electrochemical parameters, such as E_{corr}, i_{corr}, β_a, and β_c as well as the inhibitory efficiency, were calculated using varying temperatures on the corrosion of the steel area in both noninhibited and inhibited electrolytic media with the optimum concentration (10^{-3} M) of the two studied molecules (TIMQ and CDIQ), as summarized in Table 4. The results illustrated in Table 4 suggest that the corrosion current density increased as the temperature increased in a corrosive environment with and without 10^{-3} M of TIMQ and CDIQ, respectively. These increases were explained by the activation reactivity of the corrosive environment [83,84]. The findings presented in Table 4 show that the inhibition performance decreased as the temperature increased since the equilibrium on the CS surface shifted from adsorption to desorption as the temperature increased.

Table 4. PDP parameters for the steel electrode unfettered and inhibited at four temperatures in an electrolytic medium with 1 mM of the TIMQ and CDIQ molecules.

Inhibitors	Temp (K)	$-E_{corr}$ (mV/SCE)	i_{corr} (μA/cm^2)	β_a (mV dec^{-1})	$-\beta_c$ (mV dec^{-1})	η_{PDP} (%)
1 M HCl	303	456.3	1104.1	112.8	155.4	-
	313	423.5	1477.4	91.3	131.3	-
	323	436.3	2254.0	91.4	117.8	-
	333	433.3	3944.9	103.9	134.6	-
TIMQ	303	389.4	57.2	52.8	111.3	94.8
	313	405.5	110.2	65.7	159.9	92.5
	323	418.9	286.1	86.4	154.7	87.3
	333	434.9	673.8	105.2	186.1	82.9
CDIQ	303	433.4	52.1	76.6	62.0	95.2
	313	429.3	122.1	78.4	116.5	91.7
	323	421.4	235.8	84.3	163.6	89.5
	333	438.4	720.4	107.2	162.2	81.7

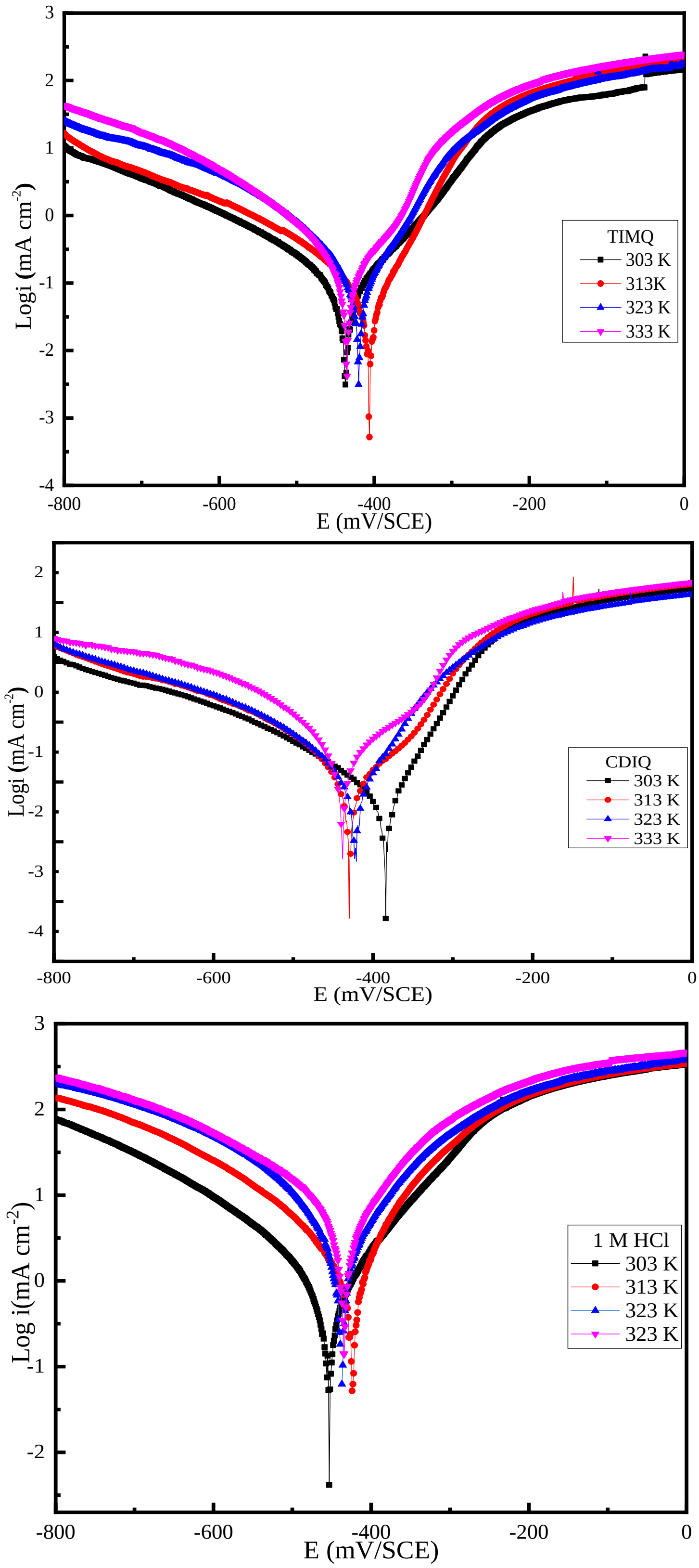

Figure 6. PDP of CS in a 1 M HCl medium with four concentrations of the inhibitors TIMQ and CDIQ at 303 K.

The investigation of the Arrhenius curves made it possible to calculate several thermodynamic parameters, namely the activation energy (E_{acv}), standard entropy variation (ΔS_{acv}) and standard enthalpy variation (ΔH_{acv}). In addition, these three parameters helped us to better understand the mechanism of action of these two products on the surface of the substrate. In addition, the thermodynamic parameters were determined according to Equations (13) and (14) [73,85].

$$i_{corr} = A\exp\left(-\frac{E_{acv}}{RT}\right) \quad (13)$$

$$i_{corr} = \frac{RT}{hN}\exp\left(\frac{\Delta S_{acv}}{T}\right)\exp\left(-\frac{\Delta H_{acv}}{RT}\right) \quad (14)$$

where i_{corr}, A, R, T, E_{acv}, and N are the current density, the Arrhenius factor, the molar gas constant, the absolute temperature, the activation energy, and Avogadro's number, respectively. Additionally, ΔS_{acv} and ΔH_{acv} denote the standard activation entropy variation and the standard activation enthalpy variation. The calculated thermodynamic parameter values are listed in Table 5. Figure 7 illustrates the logarithm of the i_{corr} (ln (i_{corr})) as a function of the 1000/temperature with and without 10^{-3} M of the two studied molecules (TIMQ and CDIQ). According to the data illustrated in Figure 7, the correlation line curve indicated that the correlation coefficient for 1 M HCl was 0.967 and the coefficients for the two elaborated molecules TIMQ and CDIQ were 0.986 and 0.971, respectively. Additionally, the E_{acv} values measured for the 1 M HCl solution and the two studied molecules TIMQ and CDIQ were 35.4, 69.8, and 71.3 kJ/mol, respectively. The activation energy values for the environments suppressed with TIMQ and CDIQ were higher than those of the blank environment, as listed in Table 5, indicating that the corrosion mechanism was altered and the steel area's corrosion was blocked by a physisorption process [72,81,86]. Furthermore, the curves of the logarithm of i_{corr}/T as a function of the 1000/T for the media no inhibited and inhibited by the two molecules TIMQ and CDIQ are illustrated in Figure 8. The study of the enthalpies $\Delta H°$ values was positive, as evidenced by the data in Table 5, which demonstrated the endothermic character of the process of adsorption and the dissolution of the steel metallic area in a corrosive environment. The ΔS_{acv} values for the no inhibited media had a negative sign, whereas the values for the media inhibited by the two examined inhibitors had a positive sign, as detailed in Table 5. Based on these findings, the speed-determining phase of the activated complex involved an association step rather than a dissociation step, increasing the order and decreasing the disorder from the environment to the activator complex [69,87,88].

Table 5. Kinetic characteristics for the steel electrode unfettered and inhibited at four temperatures in the electrolytic medium using 1 mM of the TIMQ and CDIQ molecules.

Inhibitors	R^2	E_{acv} (kJ/mol)	ΔH_{acv} (J/mol)	ΔS_{acv} (J/mol K)
HCl	0.967	35.4	32.77	−79.2
TIMQ	0.986	69.8	67.22	98.05
CDIQ	0.971	71.3	68.76	14.37

3.4. Adsorption Model

The amount of the surface (θ) covered using the adsorbed organic molecules was measured by the ratio *E*% (EIS)/100. The results were investigated graphically to adapt to various adsorption isotherm models, such as the Langmuir, Temkin, Freundluich, and Flory–Huggins models [89].

Furthermore, the C/θ plots versus the concentrations of the two studied molecules TIMQ and CDIQ provided additional information, such as a straight line with a correlation coefficient close to one (Figure 9 and Table 6). Additionally, the strong correlation due to the two studied molecules were adsorbed onto the steel metallic area, according to the Langmuir model.

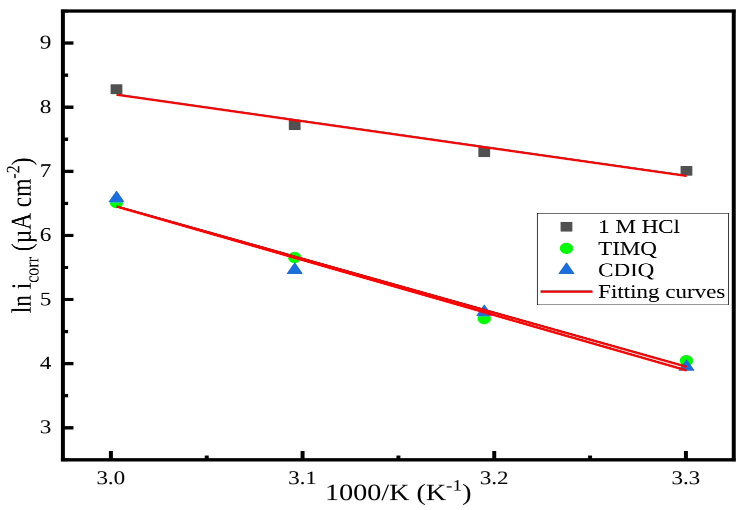

Figure 7. Logarithm of i_{corr} as a function of the 1000/T for the media uninhibited and inhibited by the two molecules TIMQ and CDIQ.

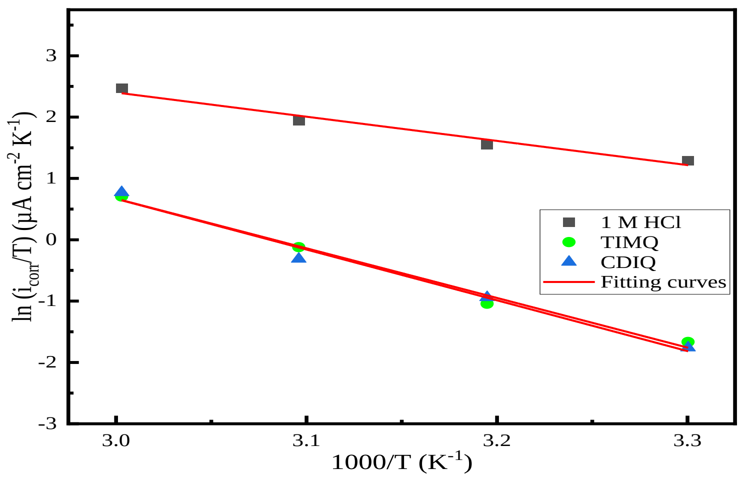

Figure 8. Logarithm of i_{corr}/T as a function of the 1000/T for the media uninhibited and inhibited by the two molecules TIMQ and CDIQ.

Table 6. Parameters of the Langmuir adsorption isotherm model for the steel electrode inhibited with 10^{-3} M of TIMQ and CDIQ molecules in the electrolytic medium.

Inhibitors	R^2	K_{ads} (L mol^{-1})	ΔG^0_{ads} (kJ mol^{-1})
TIMQ	1	1.312.10^6	−45.58
CDIQ	0.9999	5.927.10^5	−43.58

The equilibrium constant determined from the adsorption reaction were 1.312.10^6 and 5.927.10^5 L/mol, and the ΔG^0_{ads} values were −45.58 and −43.58 kJ mol^{-1}, respectively. Additionally, the ΔG^0_{ads} negative values indicated that TIMQ and CDIQ were strongly adsorbed on the CS area. The ΔG^0_{ads} values that were higher than −40 kJ/mol suggested that the two tested molecules could be adsorbed by forming the chemical bond, according to the chemisorption mode [90,91].

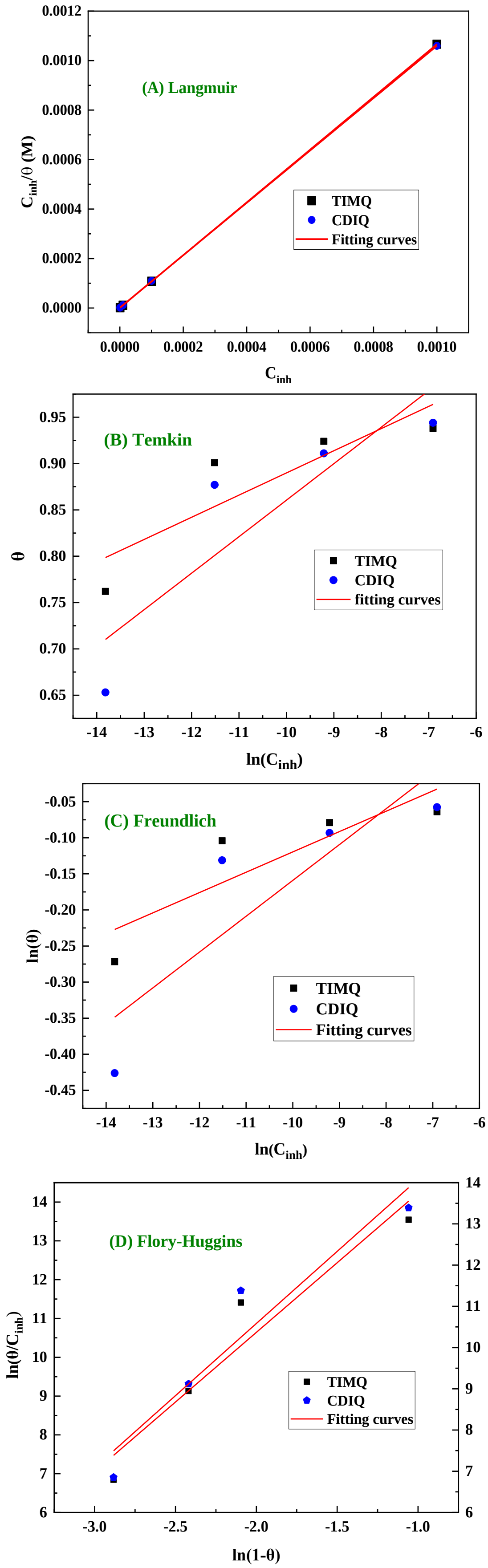

Figure 9. Langmuir (**A**), Temkin (**B**), Freundluich (**C**), and Flory–Huggins (**D**) adsorption isotherm models for CS inhibited with 10^{-3} M of TIMQ and CDIQ molecules in the electrolytic medium.

3.5. SEM/EDS Analysis

To comprehend how the surfaces of the steel samples were affected by the 1 mM concentrations of the two molecules TIMQ and CDIQ following 24 h of immersion in the electrolytic medium at 303 K, a SEM–EDS analysis was used (Figure 10) [92]. The image of the corroded steel electrode illustrated in Figure 10 shows that there were specific areas where the dezincification process was more apparent [84]. Then, in TIMQ and CDIQ that were studied at 1 mM, the heterogeneity of the steel substrates was only slightly reduced. This improvement in the morphological surface was caused by the prevention effect of the elaborate molecules (TIMQ and CDIQ) in the electrolytic medium for the steel substrate surface [92]. Further, the EDS spectra of CS alone as well as uninhibited and inhibited with 1 mM of the two studied inhibitors (TIMQ and CDIQ) after 24 h of immersion in the electrolytic medium are illustrated in Figure 10. The EDS characterization obtained for the steel substrates alone as well as uninhibited and inhibited with the two molecules at the optimal concentration is listed in Table 7. According to the results illustrated in Table 7, the data suggested that the oxygen peak for uninhibited steel substrates (21.24%) decreased with the existence of 1 mM of the two studied inhibitors TIMQ and CDIQ up to 9.45% and 16.10%, respectively. The steel substrates inhibited by the two studied inhibitors at the optimal concentration revealed that the chloride peak decreased from 3.70% to 0.78% for the uninhibited media and to 1.76% for the media inhibited by 1 mM of the two studied inhibitors TIMQ and CDIQ, respectively. These results indicated the adsorption of the TIMQ and CDIQ inhibitors onto the steel metallic surface, thus resulting in the successful protection of the steel surface against direct attack by chloride ions [84].

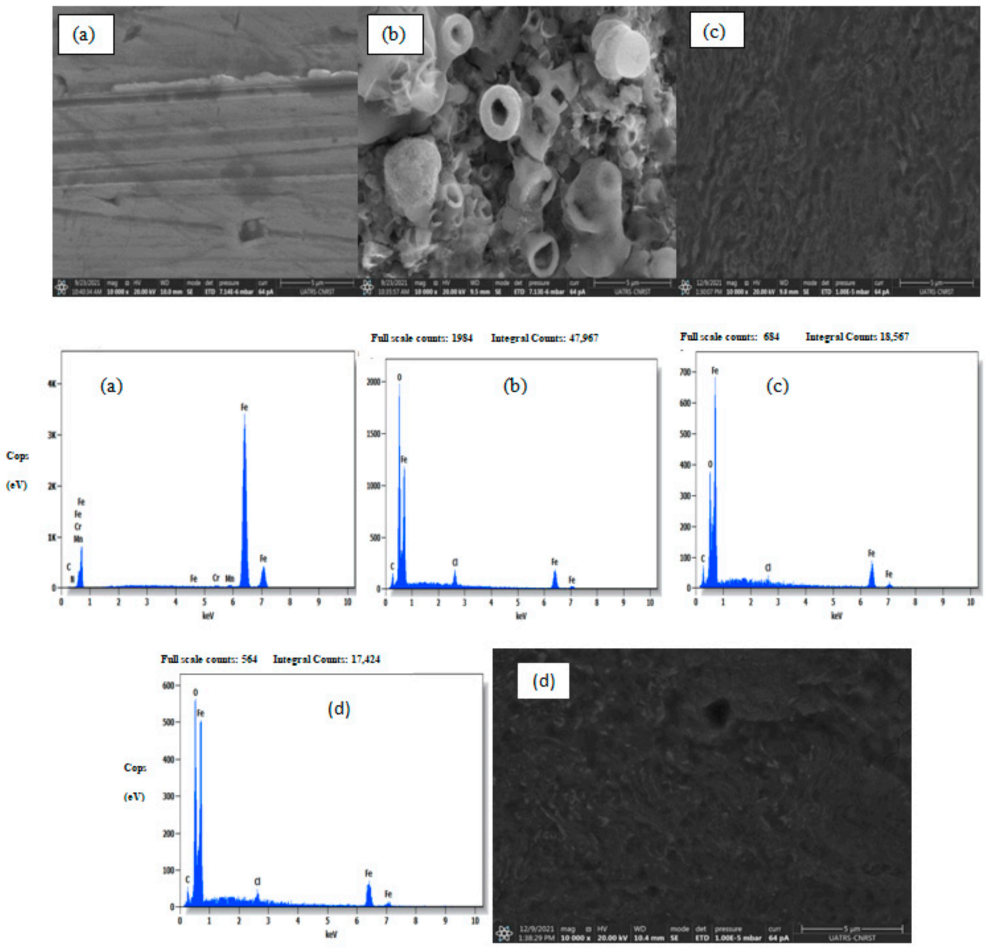

Figure 10. SEM images and EDS spectra of the CS (**a**) uninhibited (**b**) and inhibited with 1 mM of TIMQ (**c**) and CDIQ (**d**) in the electrolytic medium at 303 K.

Table 7. EDS analysis (%) of CS alone as well as uninhibited and inhibited by 1 mM of TIMQ and CDIQ in the electrolytic medium at 303 K.

Chemical Species	C (%)	N (%)	Cr (%)	Mn (%)	O (%)	Cl (%)	Fe (%)
CS Only	1.43	0.81	0.33	0.77	-	-	96.66
1 M HCl	1.40	-	-	-	21.24	3.70	73.66
10^{-3} M of TIMQ	1.62	-	-	-	9.45	0.78	88.16
10^{-3} M of CDIQ	1.27	-	-	-	16.10	1.76	80.87

3.6. UV–Visible Investigation

UV–vis testing was used to understand the behavior between the steel substrates and the tested inhibitors. The uninhibited and inhibited solutions at the optimum concentration after corrosion testing were examined (Figure 11). This method was based on the dosage of iron ions (Fe^{2+}) to calculate the difference between the number of Fe ions for the uninhibited and inhibited media with 10^{-3} M of TIMQ and CDIQ. It was shown that the number of Fe^{2+} ions decreased at the optimal concentration of the two inhibitors. Furthermore, the Fe^{2+} ions were complexed with TIMQ and CDIQ elaborated molecules. Nitrogen heteroatoms, aromatic rings, pair electron of chloride atoms, and functional alcohol were responsible for the formation of the complex. The UV–vis spectra indicated that the data was obtained according to the UV analysis with the complexation of the Fe^{2+} ions dissolved in the studied environment. According to the data illustrated in Figure 11, it was suggested that after the addition of the optimal concentration of the two studied inhibitors (TIMQ and CDIQ), the values of the wavelengths shifted towards a maximum region [68]. Additionally, the data reflected that the wavelength values appeared in a weak zone towards a maximum zone of 250 nm for the 1 M HCl solution and a maximum zone of 350 nm and 380 nm for TIMQ and CDIQ, respectively. The obtained data indicated that the two studied molecules TIMQ and CDIQ decreased the dissolution of iron ions (Fe^{2+}) in the 1 M HCl environment by forming the complex between the steel substrates and the TIMQ and CDIQ molecules [74].

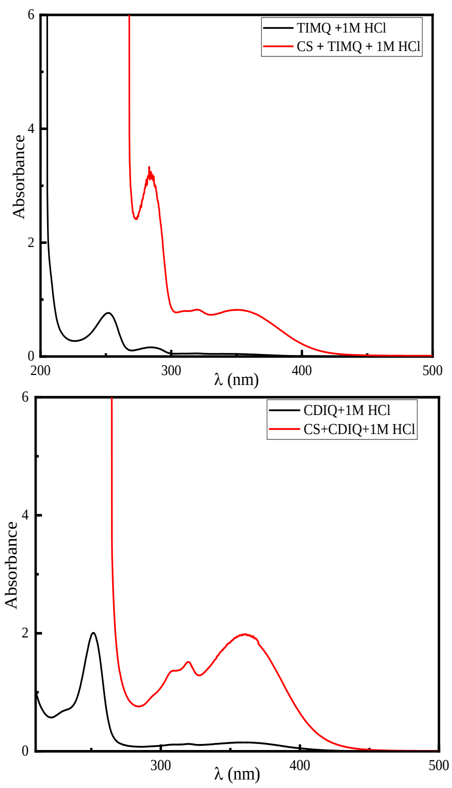

Figure 11. UV–vis spectrum for TIMQ and CDIQ in the absence and existence of CS.

3.7. DFT Results

The microspecies of these inhibitors were determined using MarvinSketch 17.1.30.0 (Chemaxon, Budapest, Hungary) as a function of pH [93] in the range of 0.0–14.0. As described in the MarviSketch manual. The most molecules contain specific functional groups that are likely to lose or gain proton(s) under specific circumstances. The equilibrium between the protonated and deprotonated forms of the molecule can be described using a constant value called pK_a. The pK_a plugin calculates the pK_a values of the molecule based on its partial charge distribution. For more details, the reader is directed to the chemaxon' webpage [94]. There are five different types of TIMQ and CDIQ inhibitors, according to the output of the Marvin Sketch software. Figure 12 shows the inhibitors' most noticeable forms, which were identified at pH = 0.00 (form 5). Form five contains the principal microspecies forms, with TIMQ and CDIQ percentages (%) of 99.99%. In this form, the two sp^2 nitrogen atoms (N1 and N3) were subjected to attack by protons in an acidic solution. Then, using this form, the theoretical computations were conducted. Additionally, for the sake of comparison, the theoretical calculations of the neutral form (form one) is also presented.

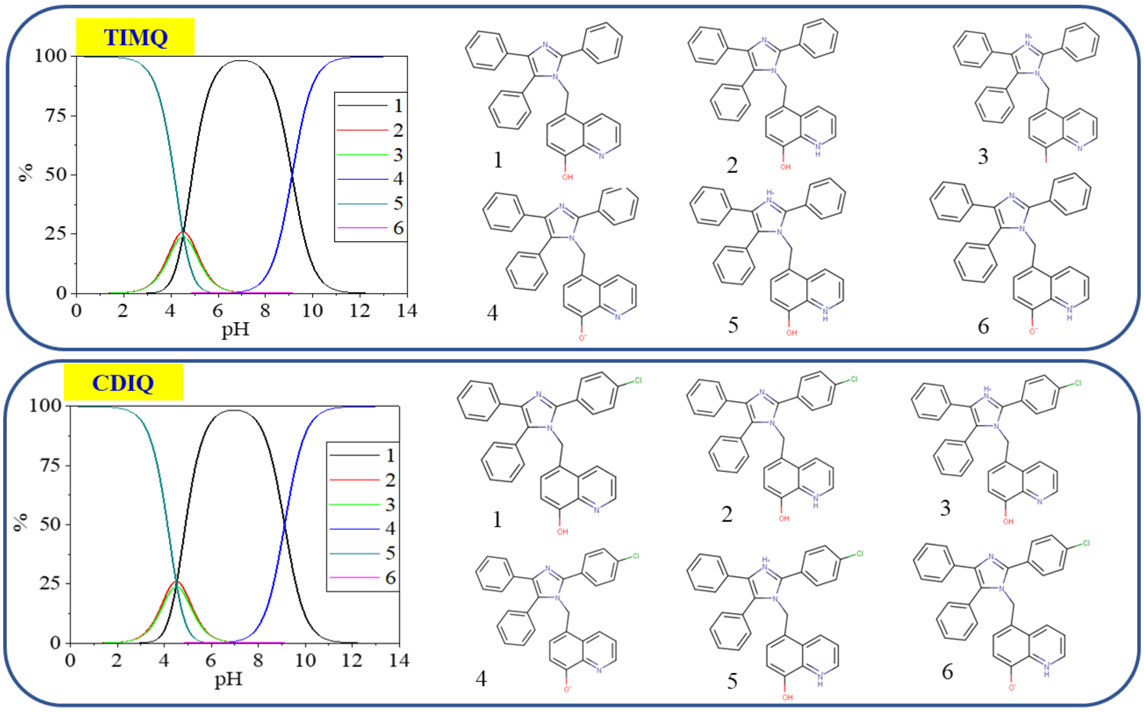

Figure 12. The microspecies percentages of the two investigated inhibitors TIMQ and CDIQ at pH = 0–14.

The two examined inhibitors' optimal geometrical structures and molecule electrostatic potential maps are shown in Figure 13. The molecular electrostatic potential (ESP) maps were utilized to qualitatively indicate and visualize the active centers that are susceptible electrophilic and nucleophilic attacks. These maps switched from a negative to a positive potential as follows: red (−Ve) < orange < green < blue (+Ve). The potential values were in the range of −0.0652 to +0.0652 au for the neutral molecules and from −0.277 to +0.277 au for the protonated species. In these maps, the negative regions (strong red color) correspond to the regions that exhibited a tendency to transfer electrons from the inhibitor to the metal surface, which were responsible for electrophilic attacks. The positive potential (blue regions) refer to the parts of the molecule that exhibited a capability to receive electrons from the metal surface, which consequently, were responsible for nucleophilic attacks [95,96]. In the neutral forms, the imine nitrogen atoms in both the pyridine and imidazole rings, as well as the π-electron of the phenyl groups, were shaded with the red color at the center, which were responsible for donating electrons to the unoccupied 3D orbitals of the Fe metal. The part of the molecules that captured electrons from the occupied 3D orbitals of the Fe metal were shaded by a dark blue color, such as some of the carbon atoms of the from the phenyl ring of the quinoline moiety. The ESP maps of the protonated forms were mostly covered by a blue color due to the protonation of the two nitrogen atoms that exhibited sp^2 hybridization. These results indicate that in acidic medium the two inhibitors could interact with the metal surface due to the donation of the π-electrons from the phenyl groups.

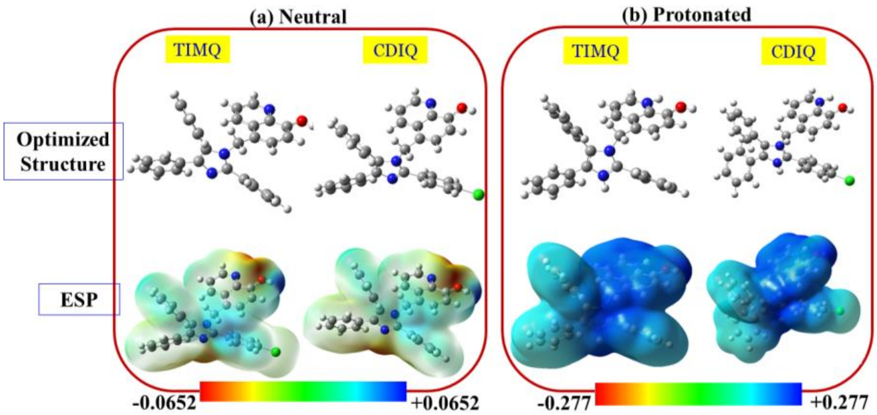

Figure 13. Optimized structures and molecular electrostatic potential maps of the two investigated inhibitors in their (**a**) neutral and (**b**) protonated forms, as obtained using the B3LYP/6-31+G(d,p) level in an aqueous solution.

The frontier molecular orbitals, FMOs (HOMO and LUMO), of the ΔE diagram of the TIMQ and CDIQ neutral and protonated forms are shown in Figure 14. As previously discussed for the ESP maps, the distribution of the HOMO surface was located at the triphenyl imidazole moiety, which contain sp^2 N atoms and delocalized π-electrons from the phenyl rings. The LUMO was distributed at the quinoline moiety of the investigated inhibitors. A similar behavior was also visualized for the protonated species. This confirmed that the imidazole, phenyl, and pyridine groups represented the parts that could contribute electrons to the metal surface. Moreover, the quinoline part of the molecule represented the segment of the molecule that could transfer electrons from the metal to form a back-donation interaction with the surface.

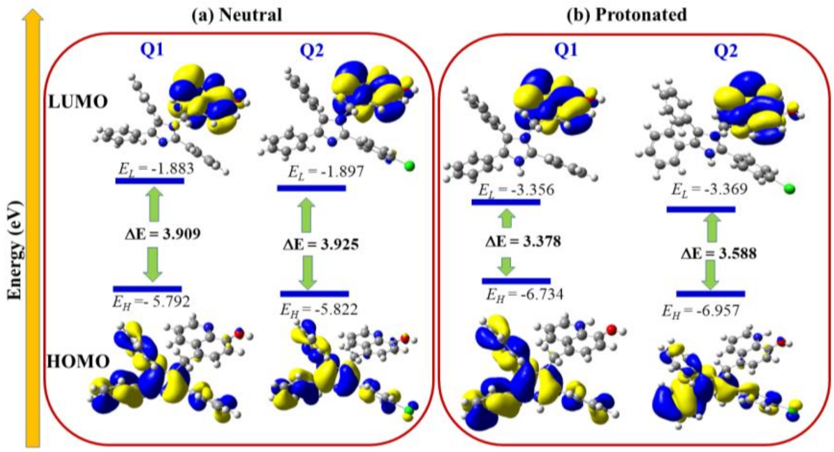

Figure 14. HOMO and LUMO molecular orbital diagrams of the TIMQ (Q1) and CDIQ (Q2) inhibitors in their (**a**) neutral and (**b**) protonated forms. The energy level diagrams of the investigated molecules are also depicted.

The quantum chemical reactivity descriptors obtained using the B3LYP/6-31+G(d,p) level of theory in an aqueous solution for the non-charged and protonated forms of TIMQ and CDIQ are regrouped in Table 8. These descriptors included the energies of the ($E(N)$, $E(N+1)$, $E(N-1)$), dipole moment (μ), energies of the frontier molecular orbitals (HOMO and LUMO), E_H and E_L, inhibitor energy gaps (ΔE), metal inhibitor energy gaps (ΔE_1 and ΔE_2), vertical ionization potential (I_v), vertical electron affinity (A_v), fundamental gap (F_g), electronegativity (χ), hardness (η), softness (S), electrophilicity (ω), fraction of electron transfer (ΔN_{110}), and back-donation energy (ΔE_{b-d}). In other words, applying an inhibitor to a metal surface helped prevent corrosion. This process involved an electron transfer between the adsorbent (metal surface) and the adsorbate (inhibitor molecule), implying an interaction of accepted-donation electrons. That is to say, one species accepted an electron, while the other donated an electron. E_H designates the propensity of a molecule to donate an electron to an acceptor species [17–19,97,98], while the E_L describes the tendency of an inhibitor to accept electrons from a donor molecule. Previous studies reported that the higher the E_H values, the easier of adsorption of molecules on the metal surface, while the lower the value of E_L, the better the inhibition potential [41,99,100]. In contrast, the energy gap (fundamental gap) is the difference between E_L and E_H (I_v and A_v) and is related to the energy barrier or gap that must be overcome before inhibition. Additionally, the ΔE is related to reactivity of the molecule. Therefore, the more reactive a molecule, the lower the ΔE (fundamental gap) value, and vice versa. In addition, within the framework of the hard and soft acid and base (HSAB), the ΔE is a descriptor than can determine the hardness and softness of the molecules. Soft molecules have a lower energy gap (and vice versa), and thus a better inhibition efficiency is expected.

Table 8. Computed quantum chemical reactivity descriptors for the investigated inhibitors in their neutral and protonated forms obtained using the B3LYP/6-31+G(d,p) level of theory in an aqueous solution.

Descriptors	Neutral		Protonated	
	TIMQ	CDIQ	TIMQ	CDIQ
$E(N)$ (Ha)	−1434.75318	−1894.3477	−1435.6498	−1895.2404
$E(N+1)$ (Ha)	−1434.82767	−1894.4227	−1435.7768	−1895.3678
$E(N-1)$ (Ha)	−1434.54517	−1894.1386	−1435.4070	−1894.9892
μ (Debye)	6.5	7.1	13.9	12.6
I_v (eV)	5.660	5.691	6.607	6.836
A_v (eV)	2.027	2.042	3.456	3.469
Eg (eV)	3.633	3.648	3.151	3.367
χ (eV)	3.844	3.866	5.031	5.152
η (eV)	1.817	1.824	1.575	1.684
S (eV^{-1})	0.550	0.548	0.635	0.594
ω (eV)	4.066	4.098	8.034	7.884
ω^+ (eV)	2.372	2.393	5.716	5.518
ω^- (eV)	6.215	6.259	10.747	10.671
$\Delta\omega$ (eV)	8.587	8.652	16.463	16.189
ΔN	0.269	0.261	−0.067	−0.099
ΔE_{b-d} (eV)	−0.454	−0.456	−0.394	−0.421
E_{HOMO} (eV)	−5.792	−5.822	−6.734	−6.956
E_{LUMO} (eV)	−1.883	−1.897	−3.356	−3.369
ΔE (eV)	3.909	3.925	3.378	3.588
ΔE_1 (eV)	6.019	6.005	4.547	4.534
ΔE_2 (eV)	5.641	5.671	6.583	6.805

The data shown in Table 8 indicated that E_H and E_L of the protonated TIMQ were higher than CDIQ. The E_L values were more in line with the experimental data provisions, compared to the E_H values. However, the ΔE of TIMQ (3.378 eV) was lower than CDIQ (3.588 eV), which did not agree with the experimental data. From the results obtained by the experiment and calculations, it can be suggested that the inhibition process using these types of inhibitors may not depend on the ease of donating electrons to the metal surface, but on the ease of accepting electrons. It is also possible to propose that the inhibition process may not be only dependent on how easily electrons migrate from the HOMO to the LUMO.

The protonated CDIQ (12.6 Debye) had a slightly larger dipole moment than TIMQ (13.9 Debye), and both of their dipole moments were greater than that of water (1.8 Debye). This indicated that CDIQ and TIMQ were able to remove water from the metal surface, preventing the corrosion of the metal. It was experimentally identified that there was no significant difference between the IE% of TIMQ and CDIQ (94.8 and 95.2%), which agreed with the computed results of the dipole moment. Hence, the two inhibitors theoretically exhibited nearly the same IE%, favoring the TIMQ inhibitor. When the other global chemical reactivity descriptors, including the electronegativity, softness, hardness, and electrophilicity, were taken into consideration, the examined inhibitors exhibited the same behavior and trend.

An important global descriptor was the ΔN from the compound to the metal surface, and vice versa. According to a report, the highest value of ΔN among a group of compounds was correlated to a strong inhibitory effectiveness. The data shown in Table 8 suggested that the two investigated inhibitors exhibited nearly similar ΔN values with a difference of 0.008 in the case of the neutral species, and 0.032 in the case of the charged form. It was also identified that the ΔN values were negative in the case of the protonated forms and positive in the case of the neutral species. The positive sign indicated that the electrons were transferred from the molecule to the metal, while the reverse was true in the case of the negative ΔN values. This change in the direction of the electron transfer was expected due to the existence of two positive charges on the two sp^2 nitrogen atoms in the protonated forms. In the case of the protonated forms, the results showed that the trend followed CDIQ > TIMQ, which agreed with the experimental findings. However, the reverse trend was observed for the neutral species.

The energy that drove the electronic back-donation process, specifically the electron transfer to the molecule and the back-donation (ΔE_{b-d}) (Equation (6)), was another measure of the global energy (Table 8). This shift in the energy suggested that the charge transfer to a molecule followed by a back-donation from the molecule was energetically preferred when $\eta > 0$ and $\Delta E_{b-d} < 0$. Therefore, the stabilization between the inhibiting molecules could be compared. This resulted in an increase in both the hardness and the interaction with the same meal. The data presented in Table 8 shows that for both forms, the order followed TIMQ > TIMQ, indicating that ΔE_{b-d} was favored for CDIQ, which agreed with the experimental data.

The energy gaps ΔE_1 and ΔE_2 were approximated using Equation (3) to explore the impact of the inhibitors on the metal surfaces. The results are recapitulated in Table 8. It was clear that the ΔE_1 referred to the electron transfer from the occupied 3*d*-Fe (Lewis acid) to the LUMO of the inhibitor (Lewis base), while the ΔE_2 corresponded to the electron transfer from the HOMO of the inhibitor (Lewis base) to the unoccupied 3*d*-Fe (Lewis acid). The values displayed in Table 8 show that, for both inhibitors, the value of ΔE_2 was significantly greater than that of ΔE_1, suggesting that the movement of electrons from the molecule with the HOMO to the unoccupied 3*d*-Fe was energetically preferable to the reverse. These results suggest that the investigated inhibitors acted similar to the Lewis acid, where ΔE_1 was smaller than ΔE_2, and the metal acted as a Lewis base. It was also found that that the order of ΔE_1 followed CDIQ < TIMQ, which indicated that the transfer of the electrons from the HOMO of the metal to the LUMO of the CDIQ (ΔE_1 = 4.534 eV) and to the metal surface was easier than the CDIQ inhibitor (ΔE_1 = 4.547 eV).

In summary, from the results of the global quantum reactivity descriptors in agreement with the experimental data, we can conclude that the two investigated inhibitors exhibited almost the same corrosion inhibition efficacy, favoring the CDIQ inhibitor. However, some descriptors showed that TIMQ was slightly more efficient than CDIQ.

3.8. Local Reactivity Descriptors (LRD)

The most relevant nucleophilic and nucleophilic Fukui functions are presented in Table 9, while the full set of results are listed in Tables S1–S4 of the Supplementary Materials. For the atomic numbers, see Figure 1.

Table 9. Selected condensed nucleophilic and electrophilic Fukui functions for the neutral and protonated forms of the investigated TIMQ and CDIQ sorted from highest (top) to lowest (down).

Neutral				Protonated			
Sites	f_A^+	**Atom**	f_A^-	**Atom**	f_A^+	**Atom**	f_A^-
TIMQ				CDIQ			
C29	0.1063	C3	0.0835	C29	0.1255	C15	0.0656
N3	0.1052	C2	0.0791	C31	0.1194	C3	0.0605
C31	0.0908	C1	0.0637	N3	0.0846	C2	0.0575
C30	0.0799	C15	0.0523	C30	0.0690	C1	0.0444
C26	0.0611	N1	0.0401	C27	0.0572	C9	0.0442
TIMQ				CDIQ			
C28	0.1046	C3	0.0824	C29	0.1251	C15	0.0762
N3	0.1033	C2	0.0782	C31	0.1192	C2	0.0668
C30	0.0894	C1	0.0635	N3	0.0844	C3	0.0561
C29	0.0789	C15	0.0519	C30	0.0691	C10	0.0524
C25	0.0607	N1	0.0397	C27	0.0569	C1	0.0463

Figure 15 shows the iso-surface representation of the nucleophilic $f^+(\mathrm{r})$ and electrophilic $f^-(\mathrm{r})$ Fukui and dual Fukui functions ($f^2(r)$ *or* $\Delta f(r)$) obtained using the equations listed in the caption of the figure. For both inhibitors, the iso-surfaces suggested that the nucleophilic attacks were centered at the imidazoline ring and the nitrogen atom of the pyridine ring. On the other hand, the electrophilic attacks occurred at the quinoline part of the molecule, especially at certain carbon atoms of the pyridine ring.

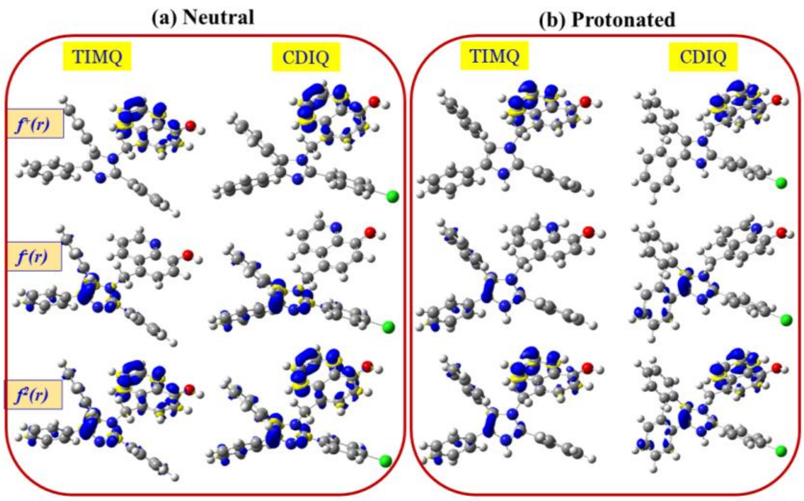

Figure 15. Nucleophilic Fukui functions $\left(f^+(\mathrm{r}) = \rho_{N+1} - \rho_N\right)$, electrophilic Fukui functions $\left(f^-(\mathrm{r}) = \rho_N - \rho_{N-1}\right)$, and the dual Fukui descriptor $\left(f^2(r) = \Delta f(r) = \rho_N - \rho_{N-1}\right)$ for (**a**) the neutral inhibitors and (**b**) the protonated inhibitors. These functions were positive, monophasic (just the blue lobes), and highlighted the sites of electrophilic and nucleophilic activity, respectively. They were produced using the finite difference algorithm (FDA) for the CV molecule. As a biphasic function, the dual descriptor revealed the electrophilic behavior ($\Delta f(r) > 0$) denoted by the blue colored lobes, and the nucleophilic behavior ($\Delta f(r) < 0$) denoted by the yellow colored lobes. The (U)B3LYP/B3LYP/H2O/PCM model was used to produce all the iso-surfaces at a pace of 0.005 au.

For the neutral species, TIMQ and CDIQ, the highest electrophilic functions resided in the C and N atoms of the imidazole ring C1, C2, and C3, while the highest active nucleophilic functions resided in the C29 and N3, which were located in the pyridine ring. For the protonated species, the highest electrophilic functions resided at the C15, C3, C2, and C1 atoms, respectively, while the highest nucleophilic functions resided at the C29, C31, and N3 centers. A comparison of the activity of the highest centers in the two inhibitors was conducted by considering the local softness and local electrophilicity. The data presented in Tables S1–S4 show that the C29, C31, and N3 centers in the protonated CDIQ inhibitor were more reactive than the analogue centers.

For a more in-depth analysis of the reactivities to nucleophilic and/or electrophilic attacks, the 3D color pie chart shown in Figure 16 highlights the double-condensed Fukui functions of the most reactive centers in protonated form. Figure 16 clearly shows that the most reactive centers responsible for nucleophilic attacks in both inhibitors were C29, C31, and N3, while those responsible for electrophilic attacks were C15 and C3. These data are in agreement with the data visualized by the ESP and the FMO.

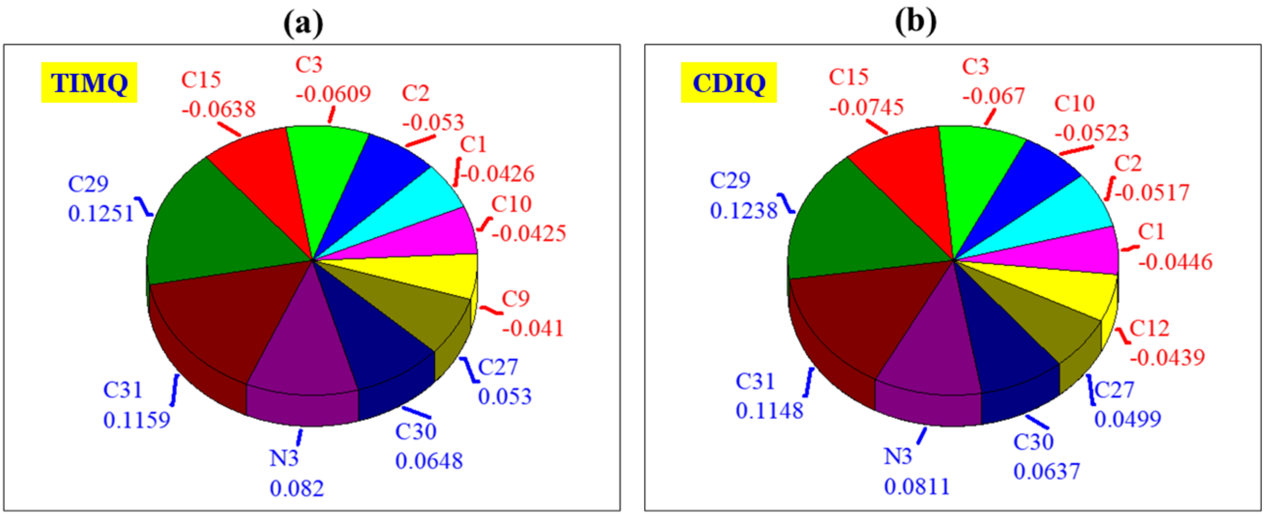

Figure 16. Color pie chart of the dual condensed Fukui functions f_A^2 for the protonated species (**a**) TIMQ and (**b**) CDIQ. The numbers in blue correspond to the negative f_A^2 values, while those in red correspond to the positive f_A^2 values.

3.9. Dynamics Simulation Study

3.9.1. Inhibitors/Fe(110)

The evaluation of the inhibitory efficacy using a theoretical MD approach was conducted to better understand the interfacial interactions between the two inhibitors TIMQ and CDIQ in both the non-charged and protonated forms and the metal substrate with the first iron layer atoms [101]. This simulation needed to account for the 303 K temperature, the acidic research media (H_3O^+, Cl^-, and H_2O), the iron metal (*Fe*(110), and the neutral and protonated TIMQ and CDIQ [102]. A low-energy arrangement was thought to be the best description for the researched inhibitors' adsorption on the metal [103,104]. Figures 17 and 18 show the photographs taken when the MDS achieved the ground state of the neutral and protonated TIMQ and CDIQ adsorbed on the surface levels of the iron atomic layers.

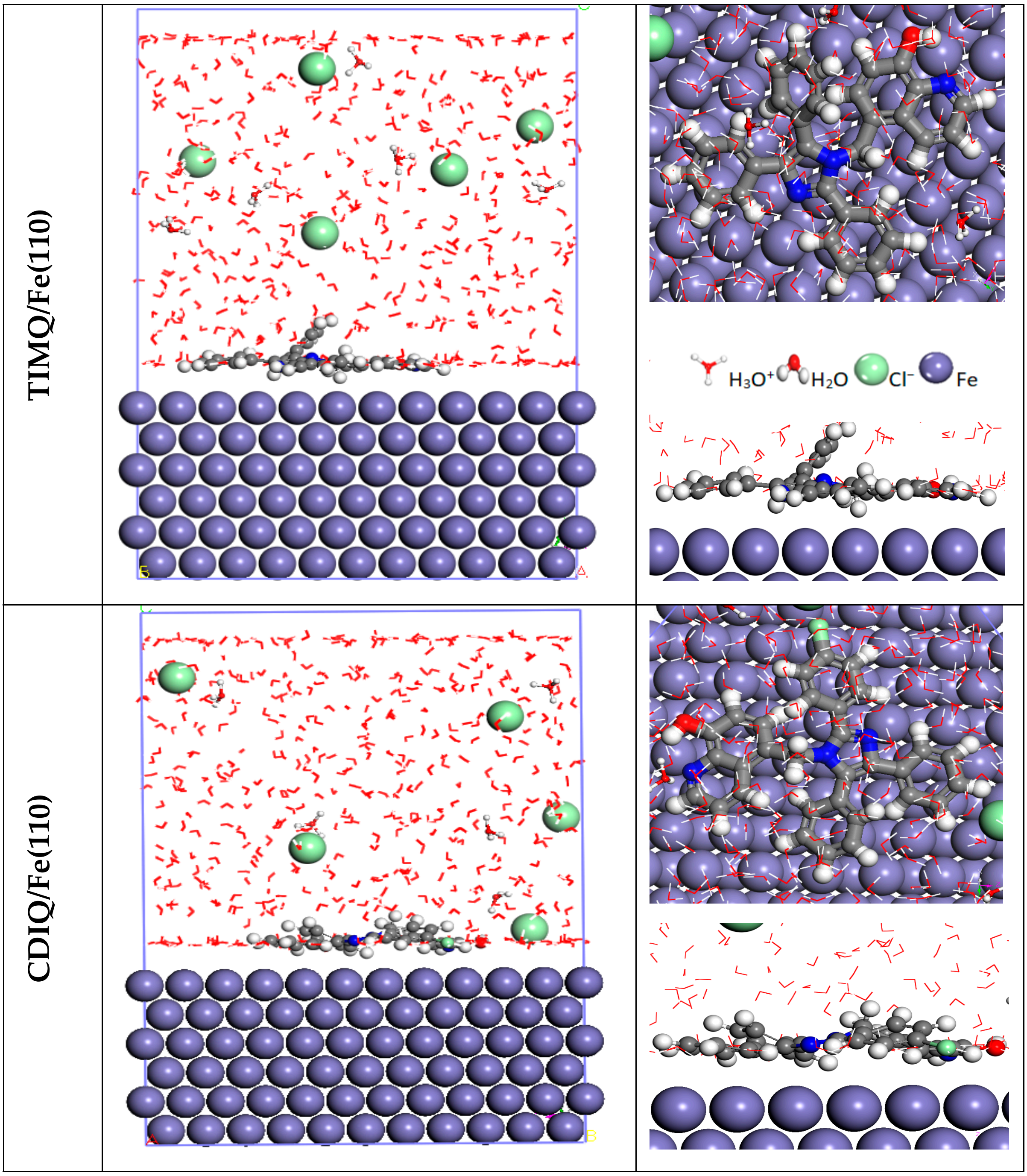

Figure 17. Images of the top and side perspectives for the TIMQ and CDIQ neutral adsorption arrangements on *Fe*(110) metal atoms.

The observed patterns in Figure 17 show that the TIMQ and CDIQ neutrals were adsorbed by the entire structure onto the investigated surface (*Fe*(110)). The simulations showed that the target molecule had a greater number of reactive centers present in the region circumscribed by the FMO densities around the *Fe* atoms, and thus had a high binding degree on the Fe area.

Concerning the adsorption of the forms carrying the double charge (Figure 18), it was axiomatic that CDIQ was completely adsorbed and parallel with the atomic support. Conversely, the neutral form TIMQ was not completely adsorbed. The quinoline base structure was adsorbed vertically and the remaining structures were completely adsorbed on *Fe*(110). This negatively affected the inhibitory performance of this form.

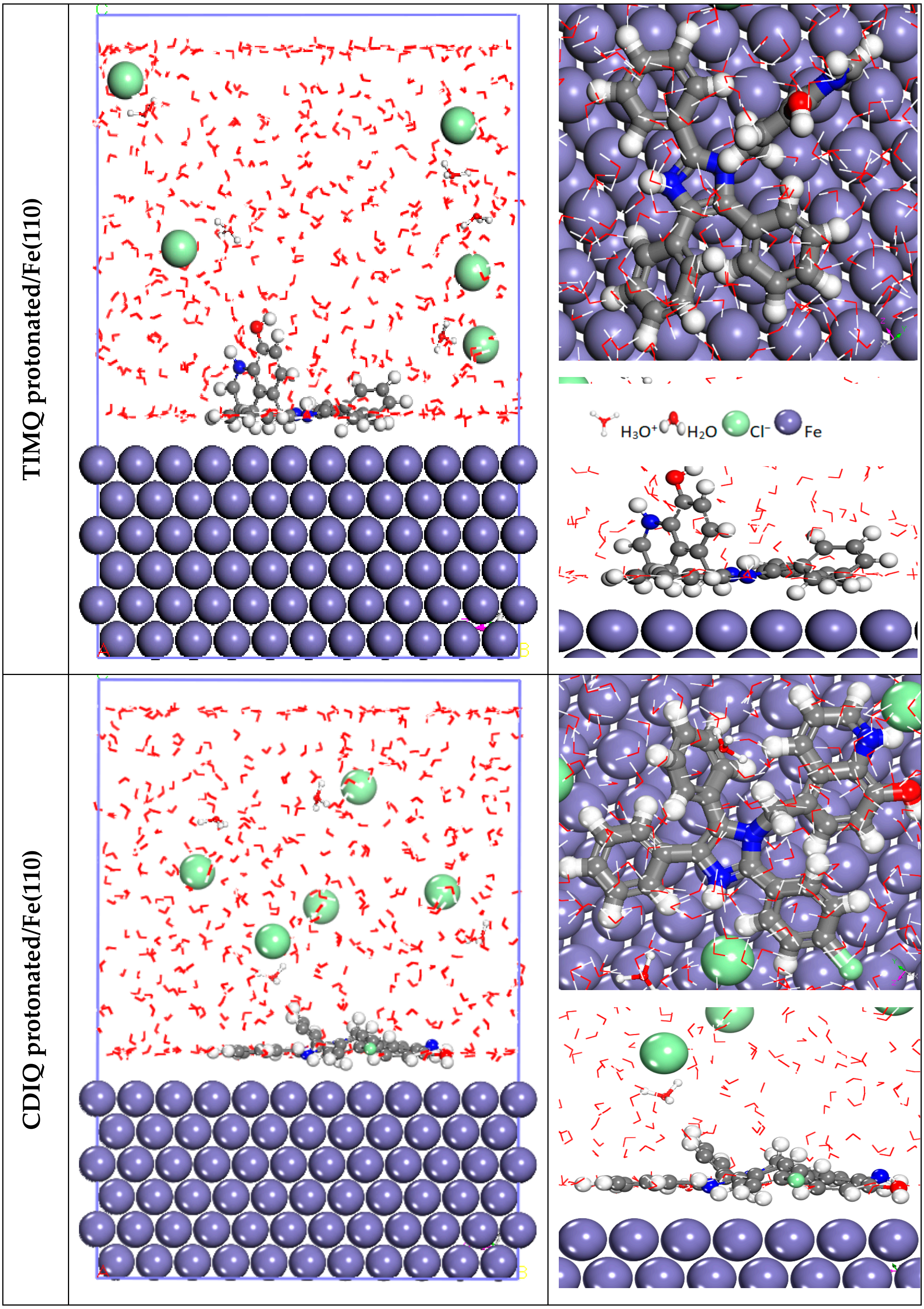

Figure 18. Pictures of the top and side views of the TIMQ and CDIQ protonated on *Fe*(110) metal atoms in their adsorption configuration.

Generally, the most stable adsorption structure had the lowest interaction energy ($E_{interaction}$) and the highest $E_{binding}$ energy. The computed values for these two energy parameters were given using the Equation (15) [105].

$$E_{interaction} = E_{total} - (E_{surface+solution} + E_{Quinoline}) \text{ and } E_{binding} = -E_{interaction} \quad (15)$$

Low $E_{interaction}$ values indicate weak interfacial contacts between the examined chemicals and the atoms of the first iron layer, whereas high $E_{binding}$ values indicate a significant adsorption [106,107]. As shown in Table 10, the quantitative data showed that the strongest $E_{binding}$ value of this system (1163.306 kJ mol^{-1}) indicated that the non-charged forms where totaly adsorbed onto the atomic layer of Fe than the protonated forms, while the most negative CDIQ neutral/*Fe*(110) value (−1163.306 kJ mol^{-1}) showed an improved CDIQ–steel surface interaction. Thus, CDIQ effectively protected the surface of the iron and strengthened the energy barrier.

Table 10. $E_{\text{interaction}}$ and E_{binding} of Quinoline/*Fe*(110), all in kJ mol^{-1}.

Systems	$-E_{\text{interaction}}$	E_{binding}
TIMQ neutral/*Fe*(110)	1146.28	1146.28
CDIQ neutral/*Fe*(110)	1163.306	1163.306
TIMQ potonated/*Fe*(110)	1100.82	1100.82
CDIQ protonated/*Fe*(110)	1151.29	1151.29

3.9.2. RDF Analysis

The main objective of this strategy was to introduce the radial distribution function ("RDF"). This evaluation is a crucial strategy used to calculate the interatomic distances between atoms, such as N1, O11, N14, and N17 for TIMQ and *Fe*, and N1, O11, N14, and N17, and Cl36 for CDIQ and iron [106]. According to the research literature, chemical adsorption is more likely when the bond length values are less than 3.5 Å. A more believable alternative is physical adsorption [108,109]. The spectral data of this analysis are represented in Figure 19. The first peak's results showed that, with the exception of N17-*Fe* (3.75 Å), the initial plane layer's neutral TIMQ and CDIQ bonds with the *Fe* atoms were shorter than 3.5 Å in length. As a result, the neutral form was tightly attached to the metallic substrate, indicating a higher inhibitory defense. The effect of the double protonation on the bond lengths led to wider distances, which decreased the inhibiting power of the proton forms against the corrosive process.

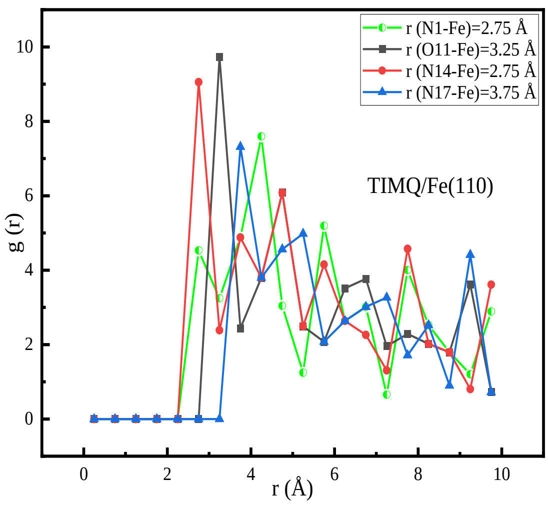

Figure 19. *Cont.*

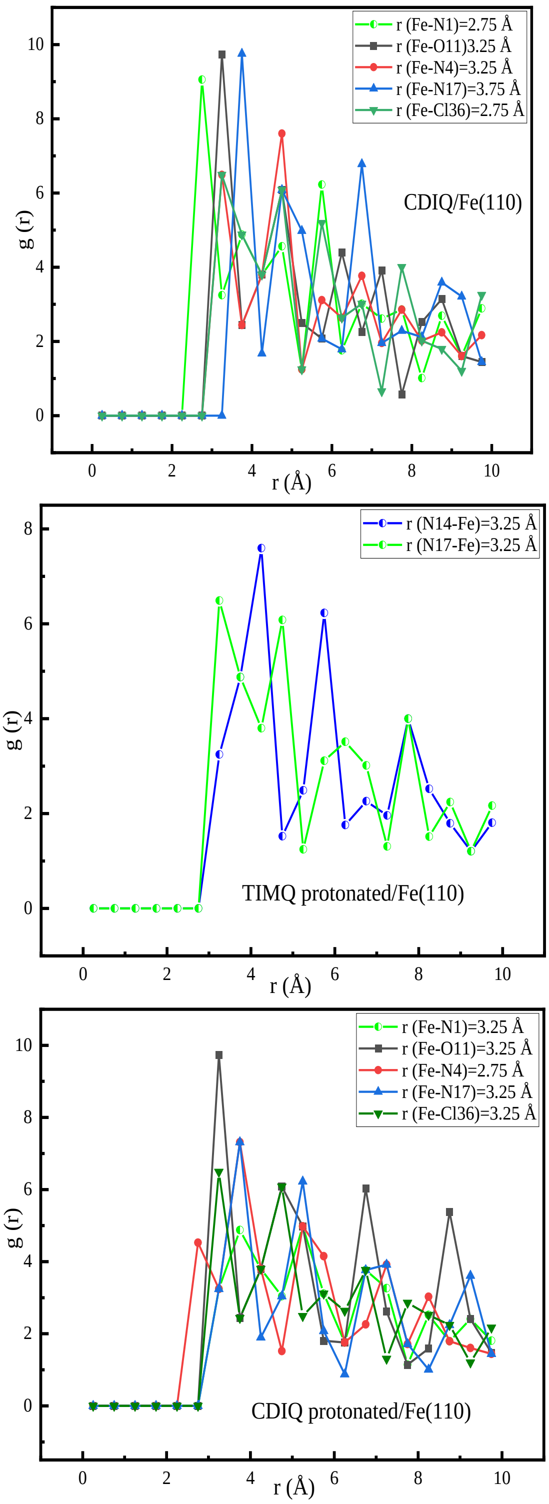

Figure 19. RDF of the TIMQ and CDIQ neutral and protonated forms on *Fe*(110) metal atoms.

In future work, we plan to study these two inhibitors in different media with different substrates in order to assess their inhibitory performance and establish a more selective and reasonable comparative study.

4. Conclusions

This study demonstrated that two classes of imidazole derivatives had an inhibitory effect for the corrosion behavior of CS specimens in a HCl medium. The inhibition efficiencies of the four inhibitor concentrations were concluded using electrochemical techniques. By using 10^{-3} M of the CDIQ in a blank solution, a +maximum corrosion inhibition efficacy of 95.8% was attained. TIMQ and CDIQ functioned as mixed-type inhibitors, according to the PDP data. The inhibitor efficiency and semicircle width increased as the inhibitor concentrations increased, according to the impedance spectra, which also showed that the inhibitor efficiency increased. The SEM/EDS analysis confirmed the surface film formation. Quantum chemical descriptors (global and local chemical reactivity) were very important for understanding that TIMQ and CDIQ inhibitors have essentially the same inhibition efficiencies, which was in agreement with the experimental data. The Fukui functions showed that the quinoline and imidazole parts were responsible for the chemical reactivity during the corrosion mechanism. In addition, the proposed inhibitors were analyzed using molecular dynamic simulations to support the adsorption process of the proposed molecules onto the CS area.

Supplementary Materials: The following supporting information can be downloaded at: https://www.mdpi.com/article/10.3390/coatings13081405/s1. Table S1: Hirshfeld charges, condensed Fukui functions (in e units), local softness in e.eV^{-1}), local electrophilicity (in e.eV) and condensed dual Fukui (in e), softness (in e.eV^{-1}) and philicity (in e.eV) descriptors for the neutral Q1 inhibitor obtained at B3lYP/6-31+G(d,p) in aqueous solution using PCM solvation model. Units "e" is the elementary charge. Table S2: As Table S1 but for the protonated form of Q1 inhibitor. Table S3: As Table S1 but for the neutral form of Q2 inhibitor. Table S4: As Table S1 but for the protonated form of Q2 inhibitor.

Author Contributions: Conceptualization, A.F.; Methodology, A.F., N.T. and M.R.; Software, A.F., N.T., Z.S.S. and H.Z.; Validation, A.F.; Investigation, A.B. (Amale Boutakiout); Resources, I.W., A.A.A., B.M.A.-M. and B.L.; Data curation, M.R., R.H., A.B. (Amale Boutakiout) and H.Z.; Writing—original draft, A.F.; Writing—review and editing, F.B. (Fouad Benhiba) and F.B. (Fouad Bentiss); Visualization, Z.S.S., I.W. and A.A.A.; Supervision, A.B. (Abdelkabir Bellaouchou), C.J., H.O. and A.Z. All authors have read and agreed to the published version of the manuscript.

Funding: This research received no external funding.

Institutional Review Board Statement: Not applicable.

Informed Consent Statement: Not applicable.

Data Availability Statement: Not applicable.

Acknowledgments: The authors extend their appreciation to the Researchers Supporting Project Number (RSP2023R381), King Saud University, Riyadh, Saudi Arabia.

Conflicts of Interest: The authors declare no conflict of interest.

References

1. Fajobi, M.; Loto, R.; Oluwole, O. Corrosion in crude distillation overhead system: A review. *J. Bio. Tribo Corros.* **2019**, *5*, 67. [CrossRef]
2. Goyal, M.; Kumar, S.; Bahadur, I.; Verma, C.; Ebenso, E.E. Organic corrosion inhibitors for industrial cleaning of ferrous and non-ferrous metals in acidic solutions: A review. *J. Mol. Liq.* **2018**, *256*, 565–573.
3. El Faydy, M.; Benhiba, F.; Warad, I.; Saoiabi, S.; Alharbi, A.; Alluhaybi, A.A.; Lakhrissi, B.; Abdallah, M.; Zarrouk, A. Bisquinoline analogs as corrosion inhibitors for carbon steel in acidic electrolyte: Experimental, DFT, and molecular dynamics simulation approaches. *J. Mol. Struct.* **2022**, *1265*, 133389.
4. Yaktini, A.E.L.; Lachiri, A.; Faydy, M.E.L.; Benhiba, F.; Zarrok, H.; Azzouzi, M.E.L.; Zertoubi, M.; Azzi, M.; Lakhrissi, B.; Zarrouk, A. Practical and theoretical study on the inhibitory influences of new azomethine derivatives containing 8-hydroxyquinoline moiety for the corrosion of carbon steel in 1 M HCl. *Orient. J. Chem.* **2018**, *34*, 3016–3029.
5. Abdallah, M.; Soliman, K.; Al Jahdaly, B.; Al-Fahemi, J.H.; Hawsawi, H.; Altass, H.; Motawea, M.; Al-Juaid, S.S. Natural parsley oil as a green and safe inhibitor for corrosion of X80 carbon steel in 0.5 MH_2SO_4 solution: A chemical, electrochemical, DFT and MC simulation approach. *RSC Adv.* **2022**, *12*, 2959–2971.
6. Laadam, G.; El Faydy, M.; Benhiba, F.; Titi, A.; Amegroud, H.; Al-Gorair, A.S.; Hawsawi, H.; Touzani, R.; Warad, I.; Bellaouchou, A.; et al. Outstanding anti-corrosion performance of two pyrazole derivatives on carbon steel in acidic medium: Experimental and quantum-chemical examinations. *J. Mol. Liq.* **2023**, *375*, 121268.

7. Ben Hmamou, D.; Salghi, R.; Zarrouk, A.; Zarrok, H.; Hammouti, B.; Al-Deyab, S.S.; Bouachrine, M.; Chakir, A.; Zougagh, M. Alizarin red: An efficient Inhibitor of C38 Steel Corrosion in Hydrochloric Acid. *Int. J. Electrochem. Sci.* **2012**, *7*, 5716–5733.
8. Ghazoui, A.; Saddik, R.; Benchat, N.; Hammouti, B.; Guenbour, M.; Zarrouk, A.; Ramdani, M. The Role of 3-Amino-2-Phenylimidazo [1,2-a]Pyridine as Corrosion Inhibitor for C38 Steel in 1M HCl. *Der. Pharma. Chem.* **2012**, *4*, 352–364.
9. Bouassiria, M.; El Faydy, M.; Benhiba, F.; Laabaissi, T.; Fakhry, H.; Saoiabi, S.; Touir, R.; Warad, I.; Guenbour, A.; Lakhrissi, B. Corrosion Effectiveness of 5-(4-Phenylpiperazin-1-yl) methyl) quinolin-8-ol for Carbon Steel in 1.0 M HCl. *J. Bio. Tribo Corros.* **2022**, *8*, 43. [CrossRef]
10. Zarrouk, A.; Hammouti, B.; Dafali, A.; Zarrok, H. L-Cysteine methyl ester hydrochloride: A new corrosion inhibitor for copper in nitric acid. *Der. Pharma. Chem.* **2011**, *3*, 266–274.
11. Zarrouk, A.; Chelfi, T.; Dafali, A.; Hammouti, B.; Al-Deyab, S.S.; Warad, I.; Benchat, N.; Zertoubi, M. Comparative Study of new Pyridazine Derivatives Towards Corrosion of Copper in Nitric Acid: Part-1. *Int. J. Electrochem. Sci.* **2011**, *5*, 696–705.
12. Zarrok, H.; Zarrouk, A.; Salghi, R.; Oudda, H.; Hammouti, B.; Ebn Touhami, M.; Bouachrine, M.; Pucci, O.H. A Combined Experimental and Theoretical Study on the Corrosion Inhibition and Adsorption Behaviour of Quinoxaline Derivative During Carbon Steel Corrosion in Hydrochloric Acid. *Port. Electrochim. Acta* **2012**, *30*, 405–417.
13. Thoume, A.; Benhiba, F.; Elmakssoudi, A.; Benmessaoud Left, D.; Benzbiria, N.; Warad, I.; Dakir, M.; Azzi, M.; Zertoubi, M.; Zarrouk, A. Corrosion inhibition behavior of chalcone oxime derivatives on carbon steel in 0.5 M H_2SO_4. *J. Appl. Electrochem.* **2021**, *51*, 1755–1770.
14. El Faydy, M.; Benhiba, F.; Warad, I.; About, H.; Saoiabi, S.; Guenbour, A.; Bentiss, F.; Lakhrissi, B.; Zarrouk, A. Experimental and theoretical investigations of two quinolin-8-ol derivatives as inhibitors for carbon steel in 1 M HCl solution. *J. Phys. Chem. Solids* **2022**, *165*, 110699.
15. Jasim, A.S.; Rashid, K.H.; AL-Azawi, K.F.; Khadom, A.A. Synthesis of a novel pyrazole heterocyclic derivative as corrosion inhibitor for low-carbon steel in 1M HCl: Characterization, gravimetrical, electrochemical, mathematical, and quantum chemical investigations. *Results Eng.* **2022**, *15*, 100573.
16. Ramachandran, A.; Anitha, P.; Gnanavel, S. Structural and electronic impacts on corrosion inhibition activity of novel heterocyclic carboxamides derivatives on mild steel in 1 M HCl environment: Experimental and theoretical approaches. *J. Mol. Liq.* **2022**, *359*, 119218.
17. Prasad, D.; Dagdag, O.; Safi, Z.; Wazzan, N.; Guo, L. Cinnamoum tamala leaves extract highly efficient corrosion bio-inhibitor for low carbon steel: Applying computational and experimental studies. *J. Mol. Liq.* **2022**, *347*, 118218.
18. Hsissou, R.; Benassaoui, H.; Benhiba, F.; Hajjaji, N.; Elharfi, A. Application of A New Tri-Functional Epoxy Prepolymer, Triglycidyl Ethylene Ether Of Bisphenol A, in The Coating Of E24 Steel In 3.5% NaCl. *J. Chem. Technol. Metall.* **2017**, *52*, 431–438.
19. Prasad, D.; Singh, R.; Safi, Z.; Wazzan, N.; Guo, L. De-scaling, experimental, DFT, and MD-simulation studies of unwanted growing plant as natural corrosion inhibitor for SS-410 in acid medium. *Colloids Surf. A* **2022**, *649*, 129333.
20. Hsissou, R.; Abbout, S.; Benhiba, F.; Seghiri, R.; Safi, Z.; Kaya, S.; Briche, S.; Serdaroğlu, G.; Erramli, H.; Elbachiri, A. Insight into the corrosion inhibition of novel macromolecular epoxy resin as highly efficient inhibitor for carbon steel in acidic mediums: Synthesis, characterization, electrochemical techniques, AFM/UV–Visible and computational investigations. *J. Mol. Liq.* **2021**, *337*, 116492.
21. Kumar, U.P.; Albrakaty, R.H.; Wazzan, N.; Obot, I.; Safi, Z.S.; Shanmugan, S.; Liang, T. Insight into the nature of the ionic interactions between some aldehydes and Ni-W alloy: A theoretical study. *Mater. Today Commun.* **2020**, *22*, 100693.
22. Obot, I.; Kaya, S.; Kaya, C.; Tüzün, B. Theoretical evaluation of triazine derivatives as steel corrosion inhibitors: DFT and Monte Carlo simulation approaches. *Res. Chem. Intermed.* **2016**, *42*, 4963–4983.
23. Obot, I.; Macdonald, D.; Gasem, Z. Density functional theory (DFT) as a powerful tool for designing new organic corrosion inhibitors. Part 1: An overview. *Corros. Sci.* **2015**, *99*, 1–30.
24. Obi-Egbedi, N.; Obot, I.; El-Khaiary, M.; Umoren, S.; Ebenso, E.E. Computational simulation and statistical analysis on the relationship between corrosion inhibition efficiency and molecular structure of some phenanthroline derivatives on mild steel surface. *Int. J. Electrochem. Sci.* **2011**, *6*, 5649–5675.
25. Costa, S.N.; Almeida-Neto, F.W.; Campos, O.S.; Fonseca, T.S.; de Mattos, M.C.; Freire, V.N.; Homem-de-Mello, P.; Marinho, E.S.; Monteiro, N.K.; Correia, A.N.; et al. Carbon steel corrosion inhibition in acid medium by imidazole-based molecules: Experimental and molecular modelling approaches. *J. Mol. Liq.* **2021**, *326*, 115330.
26. Toghan, A.; Khairy, M.; Huang, M.; Farag, A.A. Electrochemical, chemical and theoretical exploration of the corrosion inhibition of carbon steel with new imidazole-carboxamide derivatives in an acidic environment. *Int. J. Electrochem. Sci.* **2023**, *18*, 100072.
27. Hany, M.; Abd El-Lateef, K.; Shalabi Antar, A. Abdelhamid. One-pot synthesis of novel triphenyl hexyl imidazole derivatives catalyzed by ionic liquid for acid corrosion inhibition of C1018 steel: Experimental and computational perspectives. *J. Mol. Liq.* **2021**, *334*, 116081.
28. *ASTM G1*; Standard Practice for Preparing, Cleaning, and Evaluation Corrosion Test Specimens. ASTM International: West Conshohocken, PA, USA, 2003.
29. Al Garadi, W.; Jrajri, K.; El Faydy, M.; Benhiba, F.; El Ghayati, L.; Sebbar, N.K.; Essassi, E.M.; Warad, I.; Guenbour, A.; Bellaouchou, A.; et al. 4-phenyl-decahydro-1H-1,5-benzodiazepin-2-one as novel and effective corrosion inhibitor for carbon steel in 1 M HCl solution: A combined experimental and empirical studies. *J. Indian Chem. Soc.* **2022**, *99*, 100742.

30. Abd El-Lateef, H.M.; Abo-Riya, M.A.; Tantawy, A.H. Empirical and quantum chemical studies on the corrosion inhibition performance of some novel synthesized cationic gemini surfactants on carbon steel pipelines in acid pickling processes. *Corros. Sci.* **2016**, *108*, 94–110.
31. Fergachi, O.; Benhiba, F.; Rbaa, M.; Touir, R.; Ouakki, M.; Galai, M.; Lakhrissi, B.; Oudda, H.; Ebn Touhami, M. Experimental and Theoretical Study of Corrosion Inhibition of Mild Steel in 1.0 M HCl Medium by 2(-4(chloro phenyl-1H- benzo[d]imidazol)-1-yl)phenyl)methanone). *Mater. Res.* **2018**, *21*. [CrossRef]
32. Becke, A. Density-functional thermochemistry. III. The role of exact exchange. *J. Chem. Phys.* **1993**, *98*, 5648–5662.
33. Parr, R.G.; Yang, W. Density functional approach to the frontier-electron theory of chemical reactivity. *J. Am. Chem. Soc.* **1984**, *106*, 4049–4050.
34. Lee, C.; Yang, W.; Parr, R.G. Development of the Colle-Salvetti correlation-energy formula into a functional of the electron density. *Phys. Rev. B.* **1988**, *37*, 785–789. [CrossRef]
35. Yang, W.; Parr, R.G.; Pucci, R. Electron density, Kohn–Sham frontier orbitals, and Fukui functions. *J. Chem. Phys.* **1984**, *8*, 2862–2863.
36. Becke, A.D. A new mixing of Hartree–Fock and local density-functional theories. *J. Chem. Phys.* **1993**, *98*, 1372–1377.
37. Parr, R.; Yang, W. *Density-Functional Theory of Atoms and Molecules*; Oxford University Press: Oxford, UK, 1989.
38. Tomasi, J.; Mennucci, B.; Cammi, R. Quantum mechanical continuum solvation models. *Chem. Rev.* **2005**, *105*, 2999–3094.
39. Frisch, M.; Trucks, G.; Schlegel, H.; Scuseria, G.; Robb, M.; Cheeseman, J.; Petersson., G. *Gaussian 09 Revision D. 01*; Gaussian Inc.: Wallingford, CT, USA, 2009.
40. Roy, D.; Keith, T.A.; Millam, J.M. *Current Version: GaussView, Version 6*; Semichem Inc.: Shawnee Mission, KS, USA, 2016.
41. Young, D.C. A practical guide for applying techniques to real-world problems. *Comput. Chem. N. Y.* **2001**, *9*, 390.
42. Verma, D.K. Density functional theory (DFT) as a powerful tool for designing corrosion inhibitors in aqueous phase. *Adv. Eng. Test.* **2018**. [CrossRef]
43. Oubaaqa, M.; Ouakki, M.; Rbaa, M.; Ashraf, S.; Abousalem, M.; Benhiba, F.; Jarid, A.; Ebn Touhami, M.; Zarrouk, A. Insight into the corrosion inhibition of new amino-acids as efficient inhibitors for mild steel in HCl solution: Experimental studies and theoretical calculations. *J. Mol. Liq.* **2021**, *334*, 116520.
44. Guo, L.; Safi, Z.S.; Kaya, S.; Shi, W.; Tüzün, B.; Altunay, N.; Kaya, C. Anticorrosive effects of some thiophene derivatives against the corrosion of iron: A computational study. *Front. Chem.* **2018**, *6*, 155. [CrossRef]
45. Erdoğan, Ş.; Safi, Z.S.; Kaya, S.; Işın, D.Ö.; Guo, L.; Kaya, C. A computational study on corrosion inhibition performances of novel quinoline derivatives against the corrosion of iron. *J. Mol. Struct.* **2017**, *1134*, 751–761.
46. Lide, D.R. *CRC Handbook of Chemistry and Physics*, 89th ed.; CRC Press: Bocca Raton, FL, USA, 2008.
47. Gómez, B.; Likhanova, N.V.; Domínguez-Aguilar, M.A.; Martínez-Palou, R.; Vela, A.; Gazquez, J.L. Quantum chemical study of the inhibitive properties of 2-pyridyl-azoles. *J. Phys. Chem. B.* **2006**, *110*, 8928–8934. [CrossRef]
48. Ralph, G. Pearson Absolute electronegativity and hardness: Application to inorganic chemistry. *Inorg. Chem.* **1988**, *27*, 734–740.
49. Yang, W.; Parr, R.G. Hardness, softness, and the fukui function in the electronic theory of metals and catalysis. *Proc. Natl. Acad. Sci. USA* **1985**, *82*, 6723–6726. [CrossRef]
50. Parr, R.G.; Chattaraj, P.K. Principle of maximum hardness. *J. Am. Chem. Soc.* **1991**, *113*, 1854–1855. [CrossRef]
51. Özlem, U.; Gümüş, M.; Yusuf, S.; İrfan, K.; Atıf, K. Utilization of pyrazole-perimidine hybrids bearing different substituents as corrosion inhibitors for 304 stainless steel in acidic media. *J. Mol. Struct.* **2022**, *1262*, 133025.
52. Bondarev, N.V.; Katin, K.P.; Merinov, V.B.; Kochaev, A.I.; Kaya, S.; Maslov, M.M. Probing of Neural Networks as a Bridge from Ab Initio Relevant Characteristics to Differential Scanning Calorimetry Measurements of High-Energy Compounds. *Phys. Status Solidi RRL* **2022**, *16*, 2100191. [CrossRef]
53. Safi, Z.S.; Wazzan, N.; Aqel, H. Calculation of vertical and adiabatic ionization potentials for some benzaldehydes using hybrid DFT, multilevel G3B3 and MP2 methods. *Chem. Phys. Lett.* **2022**, *791*, 139349. [CrossRef]
54. Saleh, Z.A.; Taha, D.K. Calculation of Ionization energies, electron affinities, hardnesses and electro negativites, using many bases set of many methods. *Int. J. Sci. Eng.* **2014**, *5*, 727–4729.
55. Yang, W.; Mortier, W.J. The use of global and local molecular parameters for the analysis of the gas-phase basicity of amines. *J. Am. Chem. Soc.* **1986**, *108*, 5708–5711. [CrossRef]
56. Fukui, K. Role of frontier orbitals in chemical reactions. *Science* **1982**, *218*, 747–754. [CrossRef]
57. Lu, T.; Chen, F. Multiwfn: A multifunctional wavefunction analyzer. *J. Comput. Chem.* **2012**, *33*, 580–592.
58. De Proft, F.; Martin, J.M.; Geerlings, P. Calculation of molecular electrostatic potentials and Fukui functions using density functional methods. *Chem. Phys. Lett.* **1996**, *256*, 400–408.
59. Geerlings, P.; Ayers, P.W.; Toro-Labbé, A.; Chattaraj, P.K.; De Proft, F. The Woodward–Hoffmann rules reinterpreted by conceptual density functional theory. *Acc. Chem. Res.* **2012**, *45*, 683–695. [CrossRef]
60. Lee, C.; Yang, W.; Parr, R.G. Local softness and chemical reactivity in the molecules CO, SCN− and H_2CO. *J. Mol. Struct. Theochem.* **1988**, *163*, 305–313. [CrossRef]
61. *Materials Studio*; Accelrys Inc.: San Diego, CA, USA, 2016.
62. Goyal, M.; Vashisht, H.; Kumar, A.; Kumar, S.; Bahadur, I.; Benhiba, F.; Zarrouk, A. Isopentyl triphenylphosphonium bromideionic liquid as a newly effective corrosion inhibitor on metal-electrolyte interface in acidic medium: Experimental, surface morphological (SEM-EDX & AFM) and computational analysis. *J. Mol. Liq.* **2020**, *316*, 113838.

63. Andersen, H.C. Molecular dynamics simulations at constant pressure and/or temperature. *J. Chem. Phys.* **1980**, *72*, 2384–2393.
64. Hsissou, R.; Benzidia, B.; Rehioui, M.; Berradi, M.; Berisha, A.; Assouag, M.; Hajjaji, N.; Elharfi, A. Anticorrosive property of hexafunctional epoxy polymer HGTMDAE for E24 carbon steel corrosion in 1.0 M HCl: Gravimetric, electrochemical, surface morphology and molecular dynamic simulations. *Polym. Bull.* **2020**, *77*, 3577–3601.
65. Benhiba, F.; Missioui, M.; Lamghafri, S.; Hsissou, R.; Bellaouchou, A.; Oudda, H.; Lamhamdi, A.; Warad, I.; Ramli, Y.; Zarrouk, A. Theoretical and Experimental Studies of 1-Dodecyl-3-phenylquinoxalin-2(1H)-one as a Sustainable Corrosion Inhibitor for Carbon Steel in Acidic Electrolyte. *Coatings* **2023**, *13*, 1109. [CrossRef]
66. Attou, A.; Tourabi, M.; Benikdes, A.; Benali, O.; Ouici, H.B.; Benhiba, F.; Zarrouk, A.; Jama, C.; Bentiss, F. Experimental studies and computational exploration on the 2-amino-5-(2-methoxyphenyl)-1,3,4-thiadiazole as novel corrosion inhibitor for mild steel in acidic environment. *Colloids Surf. A* **2020**, *604*, 125320.
67. Hsissou, R.; Benhiba, F.; Dagdag, O.; El Bouchti, M.; Nouneh, K.; Assouag, M.; Briche, S.; Zarrouk, A.; Elharfi, A. Development and potential performance of prepolymer in corrosion inhibition for carbon steel in 1.0 M HCl: Outlooks from experimental and computational investigations. *J. Colloid Interface Sci.* **2020**, *574*, 43–60.
68. About, H.; El Faydy, M.; Benhiba, F.; Kerroum, Y.; Kaichouh, G.; Oudda, H.; Guenbour, A.; Lakhrissi, B.; Warad, I.; Zarrouk, A. Experimental and empirical assessment of two new 8-hydroxyquinoline analogs as effective corrosion inhibitor for C22E steel in 1 M HCl. *J. Mol. Liq.* **2021**, *325*, 114644. [CrossRef]
69. Hsissou, R.; Abbout, S.; Safi, Z.; Benhiba, F.; Wazzan, N.; Guo, L.; Nouneh, K.; Briche, S.; Erramli, H.; Ebn Touhami, M.; et al. Synthesis and anticorrosive properties of epoxy polymer for CS in [1 M] HCl solution: Electrochemical, AFM, DFT and MD simulations. *Constr. Build. Mater.* **2021**, *270*, 121454.
70. Thoume, A.; Elmakssoudi, A.; Left, D.B.; Benzbiria, N.; Benhiba, F.; Dakir, M.; Zahouily, M.; Zarrouk, A.; Azzi, M.; Zertoubi, M. Amino acid structure analog as a corrosion inhibitor of carbon steel in 0.5 M H2SO4: Electrochemical, synergistic effect and theoretical studies. *Chem. Data Collect.* **2020**, *30*, 100586.
71. Abbout, S.; Chebabe, D.; Zouarhi, M.; Rehioui, M.; Lakbaibi, Z.; Hajjaji, N. Ceratonia Siliqua L seeds extract as eco-friendly corrosion inhibitor for carbon steel in 1 M HCl: Characterization, electrochemical, surface analysis, and theoretical studies. *J. Mol. Struct.* **2021**, *1240*, 130611. [CrossRef]
72. El yaktini, A.; Lachiri, A.; El Faydy, M.; Benhiba, F.; Zarrok, H.; El Azzouzi, M.; Zertoubi, M.; Azzi, M.; Lakhrissi, B.; Zarrouk, A. Inhibitor effect of new azomethine derivative containing an 8-hydroxyquinoline moiety on corrosion behavior of mild carbon steel in acidic media. *Int. J. Corros. Scale Inhib.* **2018**, *7*, 609–632.
73. Hsissou, R.; Benhiba, F.; El Aboubi, M.; Abbout, S.; Benzekri, Z.; Safi, Z.; Rafik, M.; Bahaj, H.; Kaba, M.; Galai, M.; et al. Synthesis and performance of two ecofriendly epoxy resins as a highly efficient corrosion inhibition for carbon steel in 1 M HCl solution: DFT, RDF, FFV and MD approaches. *Chem. Phys. Lett.* **2022**, *806*, 139995.
74. Vengatesh, G.; Sundaravadivelu, M. Non-toxic bisacodyl as an effective corrosion inhibitor for mild steel in 1 M HCl: Thermodynamic, electrochemical, SEM, EDX, AFM, FT-IR, DFT and molecular dynamics simulation studies. *J. Mol. Liq.* **2019**, *287*, 110906. [CrossRef]
75. Laadam, G.; Benhiba, F.; El Faydy, M.; Titi, A.; Al-Gorair, A.S.; Mubark Alshareef, H.; Hawsawi, R.; Touzani, I.; Warad, A.; Bellaouchou, A.; et al. Anti-corrosion performance of novel pyrazole derivative for carbon steel corrosion in 1 M HCl: Computational and experimental studies. *Inorg. Chem. Commun.* **2022**, *145*, 109963.
76. Boumhara, K.; Harhar, H.; Tabyaoui, M.; Bellaouchou, A.; Guenbour, A.; Zarrouk, A. Corrosion inhibition of mild steel in 0.5 MH_2SO_4 solution by artemisia herba-alba oil. *J. Bio. Tribo Corros.* **2019**, *5*, 8. [CrossRef]
77. Anusuya, N.; Saranya, J.; Sounthari, P.; Zarrouk, A.; Chitra, S. Corrosion inhibition and adsorption behaviour of some bis-pyrimidine derivatives on mild steel in acidic medium. *J. Mol. Liq.* **2017**, *225*, 406–417. [CrossRef]
78. Benhiba, F.; Hsissou, R.; Benzekri, Z.; Belghiti, M.E.; Lamhamdi, A.; Bellaouchou, A.; Guenbour, A.; Boukhris, S.; Oudda, H.; Warad, I.; et al. Nitro substituent effect on the electronic behavior and inhibitory performance of two quinoxaline derivatives in relation to the corrosion of mild steel in 1M HCl. *J. Mol. Liq.* **2020**, *312*, 113367. [CrossRef]
79. Hsissou, R.; Benzidia, B.; Hajjaji, N.; Elharfi, A. Elaboration and electrochemical studies of the coating behavior of a new pentafunctional epoxy polymer: Pentaglycidyl ether pentabisphenol A phosphorus on E24 carbon Steel in 3.5% NaCl. *J. Chem. Technol. Metall.* **2018**, *53*, 898–905.
80. Hssissou, R.; Benzidia, B.; Hajjaji, N.; Elharfi, A. Elaboration, Electrochemical Investigation and morphological Study of the Coating Behavior of a new Polymeric Polyepoxide Architecture: Crosslinked and Hybrid Decaglycidyl of Phosphorus Penta methylene Dianiline on E24 Carbon Steel in 3.5% NaCl. *Port. Electrochim. Acta* **2019**, *37*, 179–191. [CrossRef]
81. Abdallah, M.; Al Bahir, A.; Altass, H.M.; Fawzy, A.; El Guesmi, N.; Al-Gorair, A.S.; Benhiba, F.; Warad, I.; Zarrouk, A. Anticorrosion and adsorption performance of expired antibacterial drugs on Sabic iron corrosion in HCl solution: Chemical, electrochemical and theoretical approach. *J. Mol. Liq.* **2021**, *33015*, 115702.
82. Benhiba, F.; Hsissou, R.; Benzekri, Z.; Echihi, S.T.; El-Blilak, J.; Boukhris, S.; Bellaouchou, A.; Guenbour, A.; Oudda, H.; Warad, I.; et al. DFT/electronic scale, MD simulation and evaluation of 6-methyl-2-(p-tolyl)-1,4-dihydroquinoxaline as a potential corrosion inhibition. *J. Mol. Liq.* **2021**, *335*, 116539. [CrossRef]
83. Molhi, A.; Hsissou, R.; Damej, M.; Berisha, A.; Bamaarouf, M. Performance of two epoxy resins against corrosion of C38 steel in 1M HCl: Electrochemical, thermodynamic and theoretical assessment. *Int. J. Corros. Scale Inhib.* **2021**, *10*, 812–837.

84. Hsissou, R.; Lachhab, R.; El Magri, A.; Echihi, S.; Vanaei, H.R.; Galai, M.; Ebn Touhami, M.; Rafik, M. Synthesis Characterization and Highly Protective Efficiency of Tetraglycidyloxy Pentanal Epoxy Prepolymer as a Potential Corrosion Inhibitor for Mild Steel in 1 M HCl Medium. *Polymers* **2022**, *14*, 3100. [CrossRef]
85. Rbaa, M.; Fardioui, M.; Verma, C.; Abousalem, A.S.; Galai, M.; Ebenso, E.E.; Guedira, T.; Lakhrissi, B.; Warad, I.; Zarrouk, A. 8-Hydroxyquinoline based chitosan derived carbohydrate polymer as biodegradable and sustainable acid corrosion inhibitor for mild steel: Experimental and computational analyses. *Int. J. Biol. Macromol.* **2020**, *155*, 645–655.
86. Fakhry, H.; El Faydy, M.; Benhiba, F.; Laabaissi, T.; Bouassiria, M.; Allali, M.; Lakhrissi, B.; Oudda, H.; Guenbour, A.; Warad, I.; et al. A newly synthesized quinoline derivative as corrosion inhibitor for mild steel in molar acid medium: Characterization (SEM/EDS), experimental and theoretical approach. *Colloids Surf. A* **2021**, *6105*, 125746.
87. El-Aouni, N.; Hsissou, R.; Safi, Z.; Abbout, S.; Benhiba, F.; El Azzaoui, J.; Haldhar, R.; Wazzan, N.; Guo, L.; Erramli, H. Performance of two new epoxy resins as potential corrosion inhibitors for carbon steel in 1MHCl medium: Combining experimental and computational approaches. *Colloids Surf. A* **2021**, *626*, 127066.
88. Echihi, S.; Hsissou, R.; Benzbiria, N.; Afrokh, M.; Boudalia, M.; Bellaouchou, A.; Guenbour, A.; Azzi, M.; Tabyaoui, M. Performance of Methanolic Extract of Artemisia herba alba as a Potential Green Inhibitor on Corrosion Behavior of Mild Steel in Hydrochloric Acid Solution. *Biointerface Res. Appl. Chem.* **2021**, *11*, 14751–14763.
89. Hsissou, R.; Abbout, S.; Seghiri, R.; Rehioui, M.; Berisha, A.; Erramli, H.; Assouag, M.; Elharfi, A. Evaluation of corrosion inhibition performance of phosphorus polymer for carbon steel in [1 M] HCl: Computational studies (DFT, MC and MD simulations). *J. Mater. Res. Technol.* **2020**, *9*, 2691–2703.
90. Berrissoul, A.; Ouarhach, A.; Benhiba, F.; Romane, A.; Guenbour, A.; Outada, H.; Dafali, A.; Zarrouk, A. Exploitation of a new green inhibitor against mild steel corrosion in HCl: Experimental, DFT and MD simulation approach. *J. Mol. Liq.* **2022**, *349*, 118102.
91. Saady, A.; Ech-chihbi, E.; El-Hajjaji, F.; Benhiba, F.; Zarrouk, A.; Rodi, Y.K.; Taleb, M.; El Biache, A.; Rais, Z. Molecular dynamics, DFT and electrochemical to study the interfacial adsorption behavior of new imidazo[4,5-b] pyridine derivative as corrosion inhibitor in acid medium. *J. Appl. Electrochem.* **2021**, *51*, 245–265. [CrossRef]
92. Benhiba, F.; Benzekri, Z.; Kerroum, Y.; Timoudan, N.; Hsissou, R.; Guenbour, A.; Belfaquir, M.; Boukhris, S.; Bellaouchou, A.; Oudda, H.; et al. Assessment of inhibitory behavior of ethyl 5-cyano-4-(furan-2-yl)-2-methyl-6-oxo-1,4,5,6-tetrahydropyridine3-carboxylate as a corrosion inhibitor for carbon steel in molar HCl: Theoretical approaches and experimental investigation. *J. Indian Chem. Soc.* **2023**, *100*, 100916.
93. Cherinka, B.; Andrews, B.H.; Sánchez-Gallego, J.; Brownstein, J.; Argudo-Fernández, M.; Blanton, M.; Bundy, K.; Jones, A.; Masters, K.; Law, D.R. Marvin: A tool kit for streamlined access and visualization of the SDSS-IV MaNGA data set. *Astron. J.* **2019**, *158*, 74.
94. Chemaxon. pKa Plugin. Available online: https://docs.chemaxon.com/display/docs/pka-plugin.md (accessed on 1 February 2019).
95. Abdel-Mottaleb, M.; Ali, S.N. A new approach for studying bond rupture/closure of a spiro benzopyran photochromic material: Reactivity descriptors derived from frontier orbitals and DFT computed electrostatic potential energy surface maps. *Int. J. Photoenergy* **2016**, *2016*, 6765805. [CrossRef]
96. Panwar, U.; Singh, S.K. Aom-based 3D-QSAR, molecular docking, DFT, and simulation studies of acylhydrazone, hydrazine, and diazene derivatives as IN-LEDGF/p75 inhibitors. *Struct. Chem.* **2021**, *32*, 337–352.
97. Ajebli, S.; Kaichouh, G.; Khachani, M.; Babas, H.; El Karbane, M.; Warad, I.; Safi, Z.; Berisha, A.; Mehmeti, A.V.; Guenbour, A. The adsorption of Tenofovir in aqueous solution on activated carbon produced from maize cobs: Insights from experimental, molecular dynamics simulation, and DFT calculations. *Chem. Phys. Lett.* **2022**, *801*, 139676.
98. Abbout, S.; Hsissou, R.; Chebabe, D.; Erramli, H.; Safi, Z.; Wazzan, N.; Berisha, A.; Reka, A.; Hajjaji, N. Investigation of Two Corrosion Inhibitors in Acidic Medium Using Weight Loss, Electrochemical Study, Surface Analysis, and Computational Calculation. *J. Bio. Tribo Corros.* **2022**, *8*, 86. [CrossRef]
99. Yu, J.; Su, N.Q.; Yang, W. Describing Chemical Reactivity with Frontier Molecular Orbitalets. *JACS Au* **2022**, *2*, 1383–1394.
100. Mehmeti, V.V.; Berisha, A.R. Corrosion study of mild steel in aqueous sulfuric acid solution using 4-methyl-4H-1, 2, 4-Triazole-3-Thiol and 2-mercaptonicotinic acid—An experimental and theoretical study. *Front. Chem.* **2017**, *5*, 61. [CrossRef]
101. Abouchane, M.; Dkhireche, N.; Rbaa, M.; Benhiba, F.; Ouakki, M.; Galai, M.; Lakhrissi, B.; Zarrouk, A.; Ebn Touhami, M. Insight into the corrosion inhibition performance of two quinoline-3-carboxylate derivatives as highly efficient inhibitors for mild steel in acidic medium: Experimental and theoretical evaluations. *J. Mol. Liq.* **2022**, *360*, 119470.
102. Benhiba, F.; Hsissou, R.; Abderrahim, K.; Serrar, H.; Rouifi, Z.; Boukhris, S.; Kaichouh, G.; Bellaouchou, A.; Guenbour, A.; Oudda, H.; et al. Development of New Pyrimidine Derivative Inhibitor for Mild Steel Corrosion in Acid Medium. *J. Bio. Tribo Corros.* **2022**, *8*, 36. [CrossRef]
103. Benhiba, F.; Sebbar, N.K.; Bourazmi, H.; Belghiti, M.E.; Hsissou, R.; Hökelek, T.; Bellaouchou, A.; Guenbour, A.; Warad, I.; Oudda, H.; et al. Corrosion inhibition performance of 4-(prop-2-ynyl)-[1,4]-benzothiazin-3-one against mild steel in 1M HCl solution: Experimental and theoretical studies. *Int. J. Hydrogen Energy* **2022**, *465*, 25800–25818.
104. Abd Allah, M.; Hegazy, M.A.; Ahmed, H.; Arej, S.; Al-Gorair, H.; Hawsawi, M.; Benhiba, F.; Warad, I.; Zarrouk, A. Appraisal of synthetic cationic Gemini surfactants as highly effi cient inhibitors for carbon steel in the acidization of oil and gas wells: An experimental and computational approach. *RSC Adv.* **2022**, *12*, 17050–17064.

105. Dutta, A.; Saha, S.K.; Banerjee, P.; Sukul, D. Correlating Electronic Structure with Corrosion Inhibition Potentiality of Some Bis-Benzimidazole Derivatives for Mild Steel in Hydrochloric Acid: Combined Experimental and Theoretical Studies. *Corros. Sci.* **2015**, *98*, 541–550.
106. Huong, D.Q.; Huong, N.T.L.; Nguyet, T.T.A.; Duong, T.; Tuan, D.; Thong, N.M.; Nam, P.C. Pivotal Role of Heteroatoms in Improving the Corrosion Inhibition Ability of Thiourea Derivatives. *ACS Omega* **2020**, *5*, 27655–27666. [CrossRef]
107. Mehmeti, V.; Podvorica, F.I. Experimental and theoretical studies on corrosion inhibition of niobium and tantalum surfaces by Carboxylated graphene oxide. *Materials* **2018**, *11*, 893.
108. El Faydy, M.; Benhiba, F.; About, H.; Kerroum, Y.; Guenbour, A.; Lakhrissi, B.; Warad, I.; Verma, C.; Sherif, E.-S.M.; Ebenso, E.E.; et al. Experimental and computational investigations on the anti-corrosive and adsorption behavior of 7-N,N′-dialkyaminomethyl-8-Hydroxyquinolines on C40E steel surface in acidic medium. *J. Colloid Interface Sci.* **2020**, *576*, 330–344. [PubMed]
109. Goyal, M.; Vashist, H.; Kumar, S.; Bahadur, I.; Benhiba, F.; Zarrouk, A. Acid corrosion inhibition of ferrous and non-ferrous metal by nature friendly Ethoxycarbonylmethyltriphenylphosphonium Bromide (ECMTPB): Experimental and MD simulation evaluation. *J. Mol. Liq.* **2020**, *3151*, 113705.